REPORT DOCUMENTATION PAGE

Public reporting burden for this collection of information is estimated to average 1 hour per response, including the time for reviewing instructions, searching data sources, gathering and maintaining the data needed, and completing and reviewing the collection of information. Send comments regarding this burden estimate or any other aspect of this collection of information, including suggestions for reducing this burden to Washington Headquarters Service, Directorate for Information Operations and Reports, 1215 Jefferson Davis Highway, Suite 1204, Arlington, VA 22202-4302, and to the Office of Management and Budget, Paperwork Reduction Project (0704-0188) Washington, DC 20503.

PLEASE DO NOT RETURN YOUR FORM TO THE ABOVE ADDRESS.

1. REPORT DATE (DD-MM-YYYY) 15-03-2003	2. REPORT TYPE Final Report	3. DATES COVERED (From – To) 01-JUN-2001 to 30-JUN-2002

4. TITLE AND SUBTITLE
Development of a Prototype Chemical Agent Detector System Based on SMO Thin Film Technology
(Final Technical Report)

5a. CONTRACT NUMBER

5b. GRANT NUMBER
N00014-01-1-0921

5c. PROGRAM ELEMENT NUMBER
01PR10038-00

6. AUTHORS
Lad, Robert J.
Tripp, Carl J.
Frederick, Brian G.
DeSisto, William

5d. PROJECT NUMBER
01342—0177

5e. TASK NUMBER

5f. WORK UNIT NUMBER
0347AM

7. PERFORMING ORGANIZATION NAME(S) AND ADDRESS(ES)
UNIVERSITY OF MAINE
OFFICE OF RESEARCH AND SPONSORED PROGRAMS
5717 CORBETT HALL
ORONO, ME 04469-5717

8. PERFORMING ORGANIZATION REPORT NUMBER
13

9. SPONSORING/MONITORING AGENCY NAME(S) AND ADDRESS(ES)
OFFICE OF NAVAL RESEARCH
BALLSTON CENTRE TOWER ONE
800 NORTH QUINCY STREET
ARLINGTON, VA 22217-5660

10. SPONSOR/MONITOR'S ACRONYM(S)
ONR

11. SPONSORING/MONITORING AGENCY REPORT NUMBER

12. DISTRIBUTION AVAILABILITY STATEMENT
Approved for Public Release

13. SUPPLEMENTARY NOTES

20030617 028

14. ABSTRACT
This research grant focused on carrying out 6.1 research activities to advance the development a next generation chemical agent detector system based on semiconducting metal oxide (SMO) technology. The tasks and the resulting findings, described in detail in this report, emphasize strategies to improve the selectivity, sensitivity, and miniaturization of the SMO detector system. Experiments were performed using organophosphonates and various alcohols as target gases. Results are reported concerning (i) selective concentration of organophosphonates on nano-sized WO_3 powders (ii) selective filtering and detection of decomposition products using catalyst-modified silica membranes (iii) kinetic signatures and decomposition reaction products associated with reactions of organophosphonates, alcohols, and ethers on WO_3 surfaces (iv) heteroepitaxial WO_3 sensing films grown on $BaF_2/Si(100)$ substrates and (vi) a dosiometer sensor based on poisonng of dispersed copper oxide nanoparticles on WO_3 films.

15. SUBJECT TERMS
chemical agent detection; SMO sensors

16. SECURITY CLASSIFICATION OF:			17. LIMITATION OF ABSTRACT	18. NUMBER OF PAGES	19a. NAME OF RESPONSIBLE PERSON
a. REPORT U	b. ABSTRACT U	c. THIS PAGE U	UU	35	Robert J. Lad
					19b. TELEPHONE NUMBER (include area code) 207-581-2257

FINAL REPORT

Development of a Prototype Chemical Agent Detector System Based on Semiconducting Metal Oxide (SMO) Thin Film Technology

Grant No.: N00014-01-1-0921
Project Period: 01-JUN-2001 to 30-JUN-2002
Budget: $460,598

Submitted By: Laboratory for Surface Science & Technology
University of Maine, 5764 Sawyer Research Center, Orono, ME 04469-5764
Phone (207) 581 – 2254; FAX (207) 581 – 2255

Submitted To: Office of Naval Research
Mr. Joe L. Brumfield, Program Officer
Ballston Centre Tower One, 800 North Quincy Street, Arlington, VA 22217-5660

1. Overview

This research grant focused on carrying out 6.1 research activities to advance the development a next generation chemical agent detector system based on semiconducting metal oxide (SMO) technology. The tasks and the resulting findings, described in detail in this report, emphasize strategies to improve the selectivity, sensitivity, and miniaturization of the SMO detector system. Experiments performed using organophosphonates and various alcohols as target gases provided the following major conclusions:

(i)   selective adsorption of organophosphonates on nano-sized WO_3 powders provides a way to selectively concentrate these compounds from the gas streams for later release to the SMO sensor element.

(ii)   silica membranes with controlled pore size and thickness, that are modified with various catalysts using atomic layer deposition, yield selective filtering and detection schemes based on detection of decomposition products.

(iii) kinetic signatures and decomposition reaction products associated with reactions of organophosphonates, alcohols, and ethers on WO_3 surfaces can be used to differentiate between these target compounds.

(iv)   heteroepitaxial WO_3 films grown on $BaF_2/Si(100)$ substrates supplied by NSWC-Dahlgren are extremely stable and offer the possibility of integrating WO_3 sensors directly onto a silicon wafer.

(vi)   dispersed copper oxide nanoparticles on WO_3 films can be used as a dosiometer sensor for organophosphorus compounds based on a phosphorus poisoning mechanism.

2. Selective Adsorption of Organophosphonates

The selective adsorption of gases on metal oxide powders is a concept used in prefiltration / concentration schemes for obtaining detection selectivity in SMO sensors. In essence, a reduction in the number of components in the gas stream impinging on the detector element is achieved through the differences in adsorption behavior and chemical reactions of gases on the surface of the adsorbate. It is also noted that this approach of selective adsorption could be used by itself or in tandem with size selective filtration strategies outlined in Section 3.

The development of filtration strategies based on selective adsorption requires a fundamental knowledge of the surface sites and chemical reactions that occur on various oxides adsorbents as well as the monoclinic WO_3 (m-WO_3) sensor element. While there is substantial literature on the surface reaction on a variety of metal oxide adsorbents, little is known about the surface sites and surface reaction of gases with WO_3-based materials. Therefore, our studies focused on determining the surface sites and the chemical reaction of organophosphonates on m-WO_3 surfaces. Our ability to synthesize high surface areas m-WO_3 particles was key to our studies as this material enabled spectroscopic detection of bands due to adsorbates. From our infrared studies on m-WO_3 particles and other oxides, we were able to develop several filtering strategies that selectively concentrate organophosponates from gas streams for later release to a sensor element.

2.1 Fabrication of nano-sized m-WO₃ powders

Little is known about the surface sites on m-WO$_3$ and surface reactions / species that occur on WO$_3$ surfaces exposed to various gases. In contrast, there is abundant literature on surface reactions occurring on other metal oxide surfaces.[1,2,3,4,5,6,7,8,9] A primary source of this data has been derived for infrared spectroscopic studies on nano-sized powders. The high surface area of the nano-particulates enables spectroscopic detection of bands due to surface bonds and adsorbed species on the surface. Similar studies on thin film oxides are difficult because the thin films typically have 3-4 orders in magnitude less surface area probed by the infrared beam. Often the powders are used as model surfaces for predicting the reactions that occur on the corresponding thin films.

In the case of m-WO$_3$, collecting infrared data on surface reactions is difficult because, to the best of our knowledge, nano-sized m-WO$_3$ powders are not commercially available. Commercial WO$_3$ powders larger than 1 μm in diameter are poor materials for infrared studies because they have a low surface area and strongly scatter the infrared beam. Given that nano-sized metal oxide particles can be used to fabricate thick film sensors, the ability to produce small particles of WO$_3$ would provide dual purposes; it would render the necessary surface area for IR studies of reactions of gaseous molecules on the surface and, at the same time, provide better nano-sized powder materials for thick film sensors.

Several synthetic approaches were used to obtain nano-sized monoclinic WO$_3$ (m-WO$_3$) powders. Details of the synthetic recipes are described in our published article.[10] All of these methods begin with a standard preparative method where H$_2$WO$_4$ is first generated by passing a Na$_2$WO$_4$ solution through a cation-exchange resin. It is found that high surface area particles are produced by dripping the H$_2$WO$_4$ exiting from the ion exchange column into a solution containing oxalate and acetate exchange ligands, or alternatively, into a water-in-oil (w/o) based emulsion. The concept of using an emulsion is illustrated in Figure 1. In essence, the polymerization and growth of the WO$_3$ particles occur in the surfactant stabilized water droplets and therefore the particle growth is dictated and limited by the size of the emulsified droplets. In comparison to commercial WO$_3$ powders, the surface area of the m-WO$_3$ powders are higher by factors of 10, and 20 times when prepared in the presence of acetate/oxalate chelating agents and w/o emulsions, respectively. The much higher surface areas enable infrared spectroscopic identification of surface sites along with detection and monitoring of gaseous reactions and adsorbed species on the surface of this metal oxide.

[1] Laperdrix, E.; Sahibed-dine, a; Costentin, G.; Bensitel, M.; Lavalley, J. *Appl. Catal. B* **2000**, 27, 137.

[2] Takeda, S.; Fukawa, M.; Hayashi, Y.; Matsumoto, K. *Thin Solid Films* **1999**, 339, 220.

[3] Smyth, D. M. *Sol. St. Ionics* **2000**, 129, 5.

[4] Kung, M. C.; Kung, H. H. *Catal. Rev.-Sci. Eng.* **1985**, 27, 425.

[5] Dobson, K. D.; McQuillan, A. J. *Spect. Acta A* **1999**, 55, 1395.

[6] Zecchina, A.; Scarano, D.; Bordiga, S.; Ricchiardi, G.; Spoto, G.; Geobaldo, F. *Catal. Today* **1996**, 27, 403.
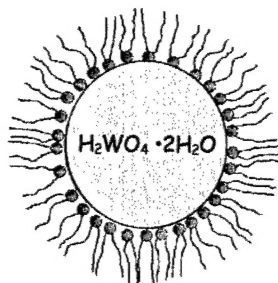
[7] Raskó, j; Novák, E.; Solymosi, f *Catal. Today* **1996**, 27, 115.

[8] Morterra, C; Magnacca, G. *Catal. Today* **1996**, 27, 497.

[9] Vuurman, M. A.; Wachs, I. E. *J. Phys. Chem.* **1992**, 96, 5008.

[10] Lu, Z.; Kanan, S. M.; Tripp, C. P. *J. Mater. Chem.* **2001**, 12, 2002.

Figure 1: Emulsion based synthesis of m-WO$_3$

Figure 2a and 2b show infrared spectra from adsorbed DMMP on thin films of commercial WO$_3$ powders and on the prepared nano-sized m-WO$_3$, respectively. The infrared spectrum of DMMP adsorbed on a nano-sized WO$_3$ powder exhibits very intense bands (see Figure 2b) whereas we do not detect any bands due to adsorbed species on the commercial powders (see Figure 2a). The amount of the adsorbed DMMP on these two WO$_3$ samples can be estimated from the diffuse reflectance infrared fourier transform (DRIFT) spectra (not shown) using the integrated peak area of the CH$_3$ mode at 1314 cm^{-1} to that of a band due to a W-O overtone mode. The amount of DMMP adsorbed on the sample (19 m^2/g) is about 15 times larger than the amount of DMMP adsorbed on the commercial powder.
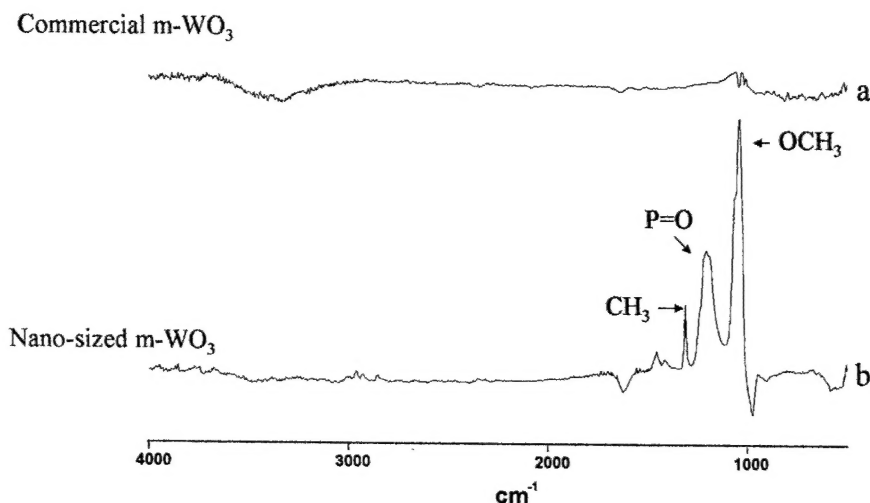
Figure 2: IR spectra of DMMP addition to a) commercial WO$_3$ and b) in-house synthesized WO$_3$.

With these higher surface area particles, it is now possible to use infrared transmission spectroscopy to monitor the reaction of gaseous molecules with the surface. The advantage of transmission using thin films is that the entire infrared region can be accessed. In the more commonly used diffuse reflectance (DRIFT), the region below 1300 cm^{-1} is not accessible because of the strong W-O fundamental bulk modes in this region. The importance of the region below 1300 cm^{-1} is shown with the adsorption of DMMP in Figure 2b. In this particular example, the O-CH$_3$ stretching modes of gaseous DMMP at 1042 and 1069 cm^{-1} did not shift upon adsorption. In contrast, the P=O stretching mode shifts from 1276 cm^{-1} in the gas phase to 1209 cm^{-1} in the adsorbed state. This shows that adsorption of DMMP on m-WO$_3$ occurs through the P=O moiety and not through the two methoxy groups.

2.2 Identification of surface sites on m-WO₃

Before embarking on gas phase adsorption studies of target and interferent molecules with these high surface area particles, there was a need to first identify the reactive groups present on the m-WO₃ surface at various evacuation temperatures. This is important because the degree of surface hydroxylation/hydration, and hence the number of exposed Lewis acid and base sites on metal oxides, can be altered by evacuation at elevated temperature. As a consequence, evacuation temperature plays a critical role in defining the surface reactions and surface species formed in subsequent reactions of gaseous molecules with the metal oxide surface.

While there are numerous infrared studies devoted to monitoring the dehydroxylation / dehydration behavior as a function of temperature on many oxides[11], we are not aware of similar studies on m-WO₃ powders. Typically, the identification of surface sites on metal oxide powders is largely based on the ability to detect infrared bands due to various hydroxyl groups (both from adsorbed water and surface M-OH modes) and by using the position of bands of adsorbed molecules such as pyridine to probe Lewis acid / Brønsted acid site densities. Bands due to adsorbed water on $WO_3 \cdot 2H_2O$ and NH_3 adsorption on sputtered tungsten oxide films have been detected,[12,13] but these studies were on amorphous WO_3 material before crystallization into the stable monoclinic form. This necessitated our studies of the hydroxylation / hydration and Lewis / Brønsted acidity of the m-WO₃ particles evacuated at different temperatures.

In terms of the dehydration of m-WO₃, Figure 3 shows DRIFT infrared spectra from a m-WO₃ sample recorded in air at room temperature (Figure 3a) and evacuated at various temperatures (Figures 3b-d). Bands located at 2063 and 1854 cm⁻¹ do not change with evacuation and are
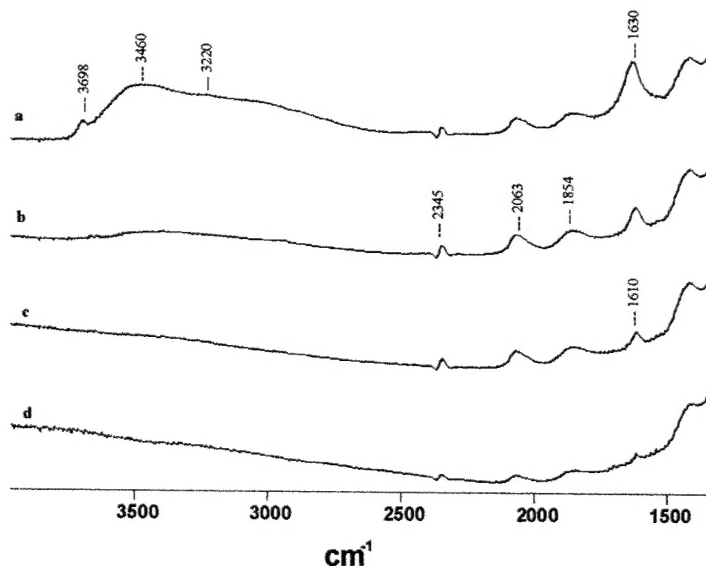
Figure 3: IR spectra of WO₃ at a) room temperature, and evacuated at b) room temperature, c) 150 °C and d) 400 °C.

[11] Morrow, B. A. In *"surface groups on oxides"*, *Spectroscopic Analysis of Heterogeneous Catalysts, Part A: Methods of Surface Analysis*; Fierro, J. L. G., ed.; Elsevier: Amsterdam, 1990.

[12] Agrawal, A.; Habibi, H *Thin Solid Films* **1989**, 169, 257.

[13] Daniel, M. F.; Desbat, b; Lassegues, J. C.; Gerand, B.; Figlarz, M. *J. Solid State Chem.* **1987**, 67, 235.

therefore assigned to various overtone and combination W-O bulk modes. The region between 3800 to 3000 cm^{-1} contains bands due to both surface WOH and adsorbed water. Since this section is devoted to dehydration and not dehydroxylation, we first describe the trends observed for the H$_2$O bending mode located at 1630 cm^{-1} because this band is unique to the presence of adsorbed water on the surface. By monitoring the change in intensity of the bending mode at 1630 cm^{-1} it is possible to determine the degree of dehydration of the m-WO$_3$ with evacuation temperature. This curve is shown in Figure 4.

The shape of the curve in Figure 4 is very similar to the weight loss curve in thermal programmed desorption experiments on amorphous hydrated tungsten hydroxy oxide (WO$_x$(OH)$_y$·H$_2$O) films.[12,14] On the amorphous material, there is a large initial decrease in weight that tapers to zero at about 150 °C followed by a second smaller decrease in weight between 300 and 350 °C. Both weight losses are due to elimination of water and it can be concluded that the initial weight loss below 150 °C is due to removal of adsorbed molecular water and the second decrease in weight beginning at 300 °C is from condensation of adjacent surface WOH groups. In our case, the data shown in Figure 4 is derived from the bending mode of water and thus, the second decrease at 350 °C is due to water removal and not WOH condensation. This shows that there are two types of adsorbed water species on the surface. Most of the adsorbed water is weakly bound to the surface and eliminated with evacuation at 150 °C. A second type of adsorbed water remains on the surface and is eliminated only after evacuation at temperatures above 350 °C.
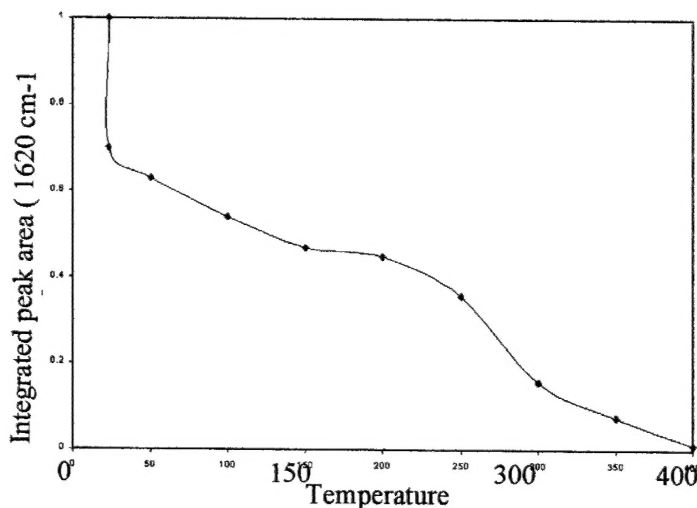
Figure 4: The amount of H$_2$O adsorbed on m-WO$_3$ as a function of evacuation temperature.

Adsorption on metal oxide surfaces occurs primarily with the surface hydroxyl groups, the adsorbed water layer and Lewis acid/base sites. On oxides such as titania and alumina, dehydroxylation leads to the creation of coordinatively unsaturated Lewis acid and base sites.[11] Pyridine is a common probe molecule to monitor the adsorption sites on metal oxide surfaces.[4,8,15,16] Adsorbed pyridine shows different and characteristic infrared bands depending

[14] Schlotter, P.; Pickelmann, L. *J. Elect. Mat* **1982**, 11, 207.
[15] Busca, G. *Catal. Today* **1998**, 41, 191.
[16] Lavalley, J. C. *Catal. Today* **1996**, 27, 377.

on whether the pyridine forms hydrogen bonds (IV), forms a pyridium ion via proton transfer with the acidic surface hydroxyl groups (V) or is coordinated to a Lewis acid site (VI). The three types of bonding are shown below.
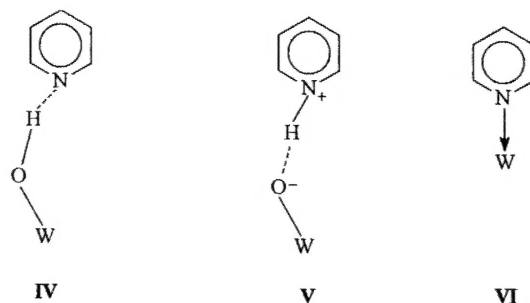
Clearly the number and type of sites will vary with the degree of dehydroxylation/dehydration of the surface. Given the dehydration behavior shown in Figure 4, we selected three evacuation temperatures of the m-WO$_3$ to be probed by the adsorbed pyridine. Specifically, the pyridine was added to a highly hydrated / hydroxylated m-WO$_3$ thin film evacuated at room temperature, and partially and fully dehydrated / dehydroxylated m-WO$_3$ samples evacuated at 150 and 400 °C, respectively.

From our pyridine adsorption studies, we found that the surface of m-WO$_3$ contains both free and hydrogen bonded hydroxyl groups as well as a layer of adsorbed water coordinated to Lewis acid sites. Both the adsorbed water and hydroxyl groups are easily removed by evacuation at 150 °C. The total number of adsorption sites are reduced by the removal of the hydroxyl groups and coordinated water, as their removal does not result in the exposure of Lewis sites on the surface. Between 150 and 400 °C the number and type of surface sites remain essentially unchanged.

2.3 Adsorption of organophosphonates on m-WO$_3$

Once we had identified the surface sites on m-WO$_3$ powders as a function of temperature, the next step was to investigate the reaction of both halogenated and non-halogenated organophosphonates with the m-WO$_3$ surface. Due to the highly toxic nature of nerve agents such as sarin and soman, our research concentrated on benign analogues of these agents. Based on a survey of the literature, dimethyl methyl phosphonate (DMMP) is by far the organophosphonate of choice for simulating the adsorption behavior of nerve agents on metal oxides.
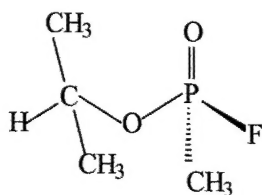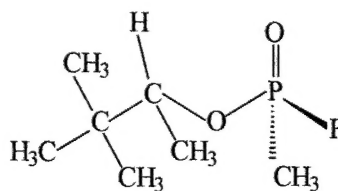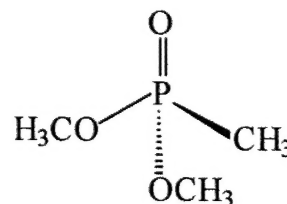
Sarin   **Soman**   **DMMP**

The desired attribute of DMMP, or any other simulant, is that it responds and behaves as close as possible to the target agents. A second obvious difference between the structure of DMMP and sarin or soman is that the nerve agents have fluorine attached to the phosphorous atom. From a toxicological point of view, sarin reacts with water producing a phosphonic acid and HF. The phosphonic acid then combines with the hydroxyl groups of esterase enzymes producing an inactive phosphonate form of the enzyme. Hydrolysis of the nerve agent may be a key factor in WO_3 based sensors as the change in conductivity upon contact with DMMP is sensitive to the humidity level of the carrier gas stream. Moreover, our infrared studies on WO_3 powders have shown that adsorbed water remains on the surface of WO_3 even after evacuation at a temperature of 350 °C. Given that nerve agents such as sarin readily hydrolyze with water or the surface water on metal oxides,[17,18] the use of a non-halogenated molecule such as DMMP may not be the best choice of molecules to mimic the sensor response of nerve agents.

The adsorption of dimethyl methylphosphonate (DMMP), trimethylphosphate (TMP), and methyldichlorophosphate (MDCP) on monoclinic tungsten oxide (m-WO_3) evacuated at various temperatures was investigated using infrared spectroscopy. In brief, we found that the adsorption of organophosphates that contain P-Cl groups differs from non-halogenated simulants such as DMMP and TMP on WO_3 surfaces. Specifically, the non-chlorinated simulants DMMP and TMP adsorb on the surface solely through the P=O functionality with the surface water layer as well as the Lewis and Brønsted acid sites. The relative number of molecules bound on Lewis and Brønsted acid surface sites depends on the initial evacuation temperature of the WO_3 surface. When MDCP adsorbs on WO_3 through the P=O bond, it is accompanied by the hydrolysis of P-Cl groups by water vapor or the adsorbed water layer leading to additional phosphate-like species on the surface. The infrared data suggest that a halogenated phosphate like MDCP is a better simulant molecule for studies aimed at understanding the role of water and hydrolysis in the response of metal oxide based sensors to nerve agents.

2.4 Adsorption of organophosphonates on silica

With our understanding of the reaction of organophosphonates on m-WO_3 in hand, our next task was to investigate the same reactions on other oxides for the purpose of identifying candidate materials for filters. On most oxides such as Al_2O_3,[19,20,21,22,23,24] TiO_2,[21,23-25] WO_3,[21,25] La_2O_3,[22] MgO,[21,22,26,27,28,29] Fe_2O_3,[22,30,31,32] and AgO,[33] DMMP adsorbs through the P=O functionality and

[17] Wagner, G. W.; Procell, L. R.; O'Connor, R. J.; Munavalli, S.; Carnes, C. L.; Kapoor, P. N.; Klabunde, K. J. *J. Am. Chem. Soc.* **2001**, *123*, 1636.

[18] Wagner, G. W.; Koper, O. R.; Lucas, E.; Decker, S.; Klabunde, K. J. *J. Phys. Chem. B* **2000**, *104*, 5118.

[19] Cao, L.; Segal, S. R.; Suib, S. L.; Tang, X.; Satyapal, S. *J. Catal.* **2000**, *194*, 61.

[20] Templeton, M. K.; Weinberg, W. H. *J. Am. Chem. Soc.* **1985**, *107*, 774.

[21] Blajeni-Aurian, B.; Boucher, M. M. *Langmuir* **1989**, *5*, 170.

[22] Mitchell, M. B.; Sheinker, V. N.; Mintz, E. A. *J. Phys. Chem.* **1997**, *101*, 11192.

[23] Rusu, C. N.; Yates Jr., J. T. *J. Phys. Chem. B* **2000**, *104*, 12292.

[24] Obee, T. N.; Satyapal, S. *J. Photochem. Photobiol., A* **1998**, *118*, 45.

[25] Kim, C. S.; Lad, R. J.; Tripp, C. P. *Sensors and Acuators A* **2001**, *76*, 441.

[26] Bertilsson, L.; Potje-Kamloth, K.; Liess, H.-D. *Langmuir* **1999**, *15*, 1128.

[27] Zhanpeisov, N. U.; Zhidomirov, G. M.; Yudanov, I. V.; Klabunde, K. J. *J. Phys. Chem.* **1994**, *98*, 10032.

[28] Li, Y.-X.; Klabunde, K., J *Langmuir* **1991**, *7*, 1388.

[29] Li, Y.-X.; Schlup, J. R.; Klabunde, K. J. *Langmuir* **1991**, *7*, 1394.

decomposes via elimination of the methoxy groups at elevated temperatures producing a stable methyl phosphonate on the surface. This is in contrast to our findings on silica. On silica, DMMP adsorbs via a hydrogen bond between the methoxy modes and the surface SiOH groups and the subsequent evacuation at elevated temperature results in the complete desorption of intact DMMP molecules from the surface.[34] Specifically, infrared spectroscopy was used to monitor the competitive adsorption / desorption behavior of the nerve gas simulants, dimethyl methylphosphonate (DMMP), trimethyl phosphate (TMP), methyl dichlorophosphate (MDCP), and trichlorophosphate (TCP) on fumed silica particles. All four compounds molecularly adsorb via hydrogen bonds (H-bonds) with the surface hydroxyl groups. The adsorption strength depends on two factors: the specific functional group H-bonded to the surface hydroxyl groups and the number of such bonds per molecule.

From pair-wise competitive adsorption studies we find that there is a high degree of selectivity of adsorption of one type of phosphonate over another class of phosphonate. For example, when a silica sample pretreated with MDCP is exposed to single 20 seconds exposure to excess DMMP, the adsorbed MDCP is expelled and the silica surface contains only adsorbed DMMP. In the reverse experiment, pre-adsorbed DMMP is not removed by exposure to excess MDCP. Furthermore, when a 1:1 MDCP/DMMP mixture is exposed to a bare silica sample, again spectral features only due to adsorbed DMMP are detected. This high degree of selective adsorption between DMMP and MDCP is mirrored when the same sets of experiments are performed for DMMP verses TMP. In this case, TMP is selectively adsorbed over DMMP. Collectively, the high degree of selectivity derived from the competitive adsorption involving TCP, MDCP, DMMP and TMP demonstrate the potential selectivity when using chemical displacers. This degree of selectivity is not obtained using thermal desorption based methods.

We have shown that by judiciously selecting chemical displacers as dictated by the two factors, (i.e., type and number of functional groups H-bonded to the surface silanols) it is possible to selectively and sequentially dislodge each of the four phosphonate compounds adsorbed on silica. The number of functional groups adsorbing on the surface is determined by the structure of the adsorbate whereas the strength of the H-bond can be estimated from the shift in the infrared SiOH stretching mode at 3747 cm^{-1}. The stronger the H-bond, the greater the shift in the SiOH band, and these are listed for various functional groups in Table 1.

Based on the relative adsorption strength of the phosphonates on silica and the data from Table 1, it is possible to construct a generalized scheme for the selection of appropriate adsorption strength required for each chemical displacer (labeled A, B, and C).

TCP < DCMP < Displacer A < DMMP < Displacer B < TMP < Displacer C

Over 20 compounds were tested in order to identify suitable compounds for displacer A, B and C. The relative effectiveness of each displacer molecule was deduced from pair-wise competitive adsorption studies in which infrared spectroscopy was used to identify the number

[30] Hedge, R. I.; White, J. M. *Appl. Surf. Sci.* **1987**, 28, 1.

[31] Henderson, M. A.; Jin, T.; White, J. M. *J. Phys. Chem.* **1986**, 90, 4607.

[32] Tesfai, T. M.; Sheinker, V. N.; Mitchell, M. B. *J. Phys. Chem. B* **1998**, 102, 7299.

[33] Taranenko, N.; Alarie, J.-P.; Stokes, D. L.; Vo-Dinh, T. *J. Raman Spectrosc.* **1996**, 27, 379.

[34] Kanan, S. M.; Tripp, C. P. *Langmuir* **2001**, 17, 2213.

Table 1. Shift in frequency of the SiOH stretching mode at 3747 cm^{-1} after the adsorption of the following compounds.

Compound	V_{OH}	Compound	V_{OH}
n-C_6H_{14}	3701	Acetone	3402
Cyclohexane	3699	Cyclopentanone	3372
CCl_4	3690	Cyclohexanone	3348
Benzene	3688	1,4-dioxane	3327
CH_3NO_2	3683	t-Butanol	3325
CH_3CN	3670	2-cyclohexene-1-one	3324
H_2CO	3493	*TMP*	**3262**
TCP	**3488**	$(C_2H_5)_2O$	3230
CH_3OH	3470	*DMMP*	**3223**
CH_3CHO	3447	Tetrahydrofuran	3205
MDCP	**3425**	Pyridine	2830
$CH_3CO_2C_2H_5$	3411	Triethylamine	2667

and type of adsorbed molecules on the silica surface. From this work, suitable displacer molecules were identified as A= triethylamine (TEA), B= 2-Pyridyl acetonitrile(2-PyAN) and C= ethylene diamine (EDA).
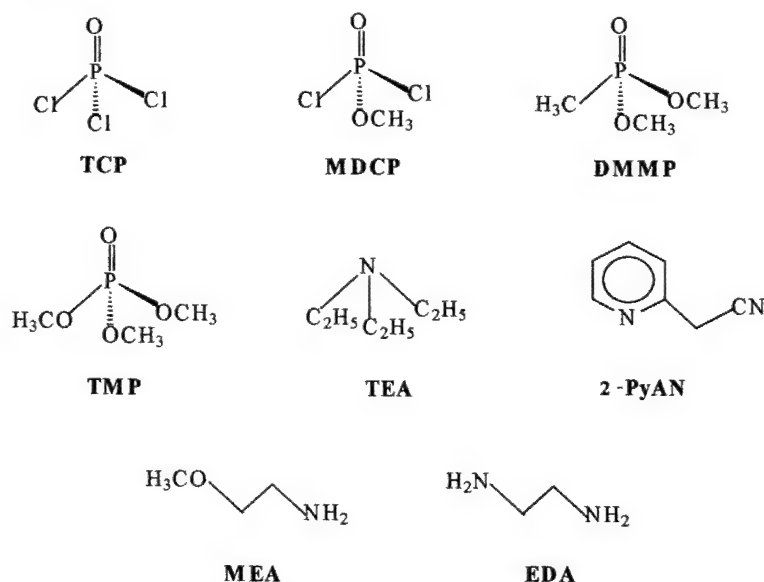

Chart 1 illustrates the structural formulas of these compounds.

These results led to a novel filtering strategy scheme.   Based on the identification of suitable molecules for displacers A-C, it is now possible to construct possible schemes for the selective

chemical displacement of the 4 classes of organophosphonates from silica. One strategy would involve sequential addition of the chemical displacers (see Scheme 1). In the first step TMP, DMMP and DCMP would be concentrated on silica and separated from TCP by passing the gas stream through a silica filter.

A TEA pulse would then pass through the silica and the effluent gas stream would contain the displaced MDCP and excess TEA. Subsequent removal of the TEA from the MDCP/TEA mixture could be accomplished by passing the mixture through an acid filter converting the TEA to a nonvolatile salt. In a similar manner, sequential pulses of 2-PyCN would be used to displace DMMP followed by an EDA to finally remove TMP. In this strategy, the amine chemical displacers would be added to the gas stream and would have to be separated by inserting and additional filter to remove the amines.

An alternative filtering strategy could be used to avoid generating amines in the gas stream. This is depicted in Scheme 2. The first filter the gas stream would encounter silica pretreated with 2-PyCN. TMP would selectively adsorb liberating a small amount of 2PyCN in the process. The
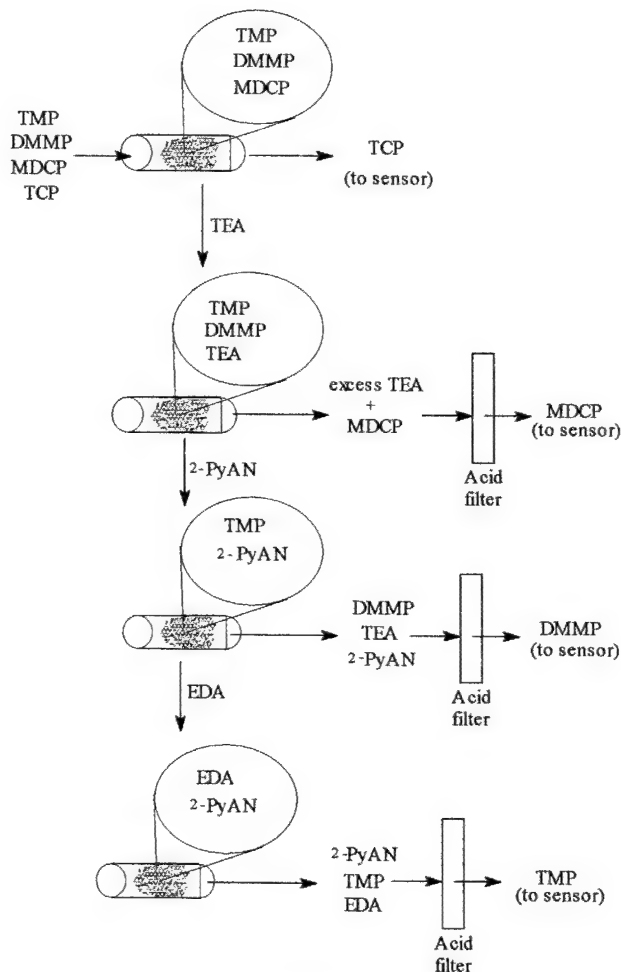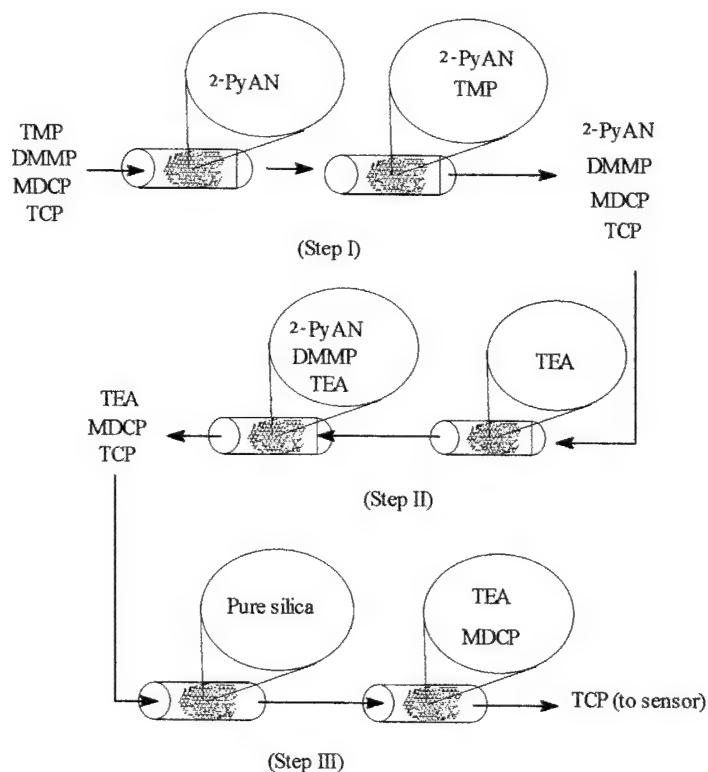

Scheme 1

gas stream would then pass through a silica filter doped with TEA. DMMP and 2-PyCN would adsorb liberating some TEA. Finally, the gas stream would pass through silica where DCMP and TEA would adsorb. TCP would pass through the silica and be detected separately. In this configuration, each filter now contains one phosphonate and an adsorbed amine. HCl vapor could then be added to convert the amines to salts and the phosphonates would then be released by applying a thermal pulse.

The feasibility of extending this approach to G-agents was probed. Specifically, a computational tool was developed for predicting filtering strategies for toxic nerve agents. Using *ab initio* calculations it was possible to directly correlate the calculated partial charge on the methoxy oxygen atoms based on Mulliken population analysis with the adsorption strength of six simulant phosphonate molecules on a silica surface. Therefore, we are confident that we have a predictive tool that will be a key enabler for extending our current and future filtering strategies based on simulant data to their toxic analogues. Calculations for GA, GB and GD have led us to identify appropriate displacer molecules to selectively displace each toxic agent from a silica surface. We have filed a US patent on this work.

The schemes described here demand some estimate of the relative adsorption strength of the live agents on silica. For example, sarin ($O=PF(CH_3)(OCH_3)$) contains 1 methoxy group and thus we expect it to be more weakly adsorbed than DMMP. An estimate on the strength of the H-bond between the methoxy group of sarin and the surface SiOH groups can be deduced from AMI

Scheme 2

semi-empirical calculations. Table 2 lists the partial charge on the methoxy oxygen atoms based on Mulliken population analysis. There is good correlation with the magnitude of the charge on the oxygen atom and the shift in the SiOH band of silica for MDCP, DMMP and TMP. For example, the calculated values correctly position the H-bond strength of DMMP higher than the H-bond strength of TMP. Based on these calculations, we would expect that the adsorption strength of sarin would lie between MDCP and DMMP. The adsorbed strength would be slightly stronger than MDCP and on the same order as the individual H-bond for DMMP. Thus, we expect sarin to adsorb onto silica shifting the SiOH band to near 3223 cm^{-1} and that it would be displaced by TEA.

Table 2. Partial charges on the methoxy oxygen atoms based on Mulliken population analysis.

Compound	Charges of the Methoxy Oxygen Atoms
MDCP	-0.635
DMMP	-0.734, -0.775
TMP	-0.707, -0.745, -0.745
Sarin	-0.775

2.5 Attachment of filter layer to an active sensor element

The next technical hurdle to implementation of this filtering approach requires the development of methods for anchoring the silica filter on top of the active sensor element. In our first approach, we investigated the use of Atomic Layer Deposition (ALD) in which separate gas streams containing SiCl$_4$ and water are sequentially exposed to the WO$_3$ surface. By using infrared spectroscopy to follow the reaction, we found that it is possible to chemically grow a high surface area silica layer on top of WO$_3$ surface one layer at a time. In particular, it is found that a minimum of three complete cycles (SiCl$_4$, then water) is required to achieve full coverage of the WO$_3$ with a silica layer. It is found that the ALD silica layer only acts as a filter when it is not calcined at elevated temperature. The addition of DMMP to silica coated WO$_3$ powder that was pretreated by calcination at 400°C does not lead to any filtering of the DMMP. In this case, the DMMP adsorbs directly on the WO$_3$. However, when DMMP is exposed to a silica coated WO$_3$ powder that has not been calcined at 400°C, the DMMP selectively concentrates on the silica. Subsequent application of a thermal pulse results in the transfer of the DMMP from the silica to the WO$_3$. We speculate that the calcination step leads to shrinkage of the silica layer exposing the underlying WO$_3$ surface.

3. Microporous Membranes

A significant issue in furthering the progress of SMO sensors is improving their selectivity between similar classes of analytes. In this part of the research, two methods were investigated for enhancing selectivity for sensing gaseous organophosphonate compounds.

The first method focused on developing mesoporous and microporous thin films of silica that act as membranes for separating incoming complex gas streams prior to contacting the active sensor material. Controlling the pore size and thickness of the silica membrane enables the separation of a wide variety of gas mixtures. Work entailed preparing and characterizing cubic mesoporous membranes for gas separation. It is important to note that these membranes were prepared on porous substrates in order to fully characterize their gas separation capability. In addition to mesoporous membranes, an atomic layer deposition reactor was constructed to further modify the mesoporous membranes and enhance their gas separation capabilities.

The second method focused on preparing thin composite films of platinum/silica tailored to ultimately sense sarin gas. Platinum is known to catalyze the hydrolysis of sarin to form hydrofluoric acid, and hydrofluoric acid is a well known selective etch for silica. Allowing these two, highly selective, successive steps to occur potentially provides a sensor that is highly selective to sarin. The first step in achieving such a sensor was preparing a thin composite film of platinum/silica by chemical vapor deposition. The films were characterized by x-ray diffraction, x-ray photoelectron spectroscopy and thickness measurements. An interesting discovery involved the catalytic decomposition of the silica precursor by the platinum precursor. Infrared spectroscopy was used to examine this catalytic decomposition.

3.1 Fabrication of 3-dimensional cubic mesoporous membranes

Three-dimensional cubic mesoporous silica membranes were prepared by micellular templating techniques. Both the hydrothermal and dip-coated membranes were deposited on macroporous α-alumina support disks having an average pore diameter of 1 μm and porosity of 35%, as measured by Hg porosimetry.

The hydrothermal membranes were made by placing the support in tetraethylorthosilicate (TEOS). Then a solution consisting of H_2O, NaOH and Cetyltrimethyl-ammonium bromide (CTAB) was added to the support/TEOS. The final molar ratio of the reaction mixture was 1 TEOS/ $61H_2O$/ 0.5 NaOH/ 0.59 CTAB. The solution + support was stirred in a beaker until it became inhomogeneous. The reaction mixture and support were then autoclaved at 95°C followed by calcination at 500°C. After calcination the membrane was polished to remove excess SiO_2 from the surface.

The dip coated membranes were fabricated by first synthesizing a TEOS sol. The sol was made with molar ratios of 1 TEOS/ 3 EtOH/ 1 H_2O/ $5x\ 10^{-5}$ HCl. The dipping solution was made by adding ethanol, water, HCl and CTAB to the prehydrolized sol. The final molar ratios of the dipping sol were 1 TEOS/ 20 EtOH/ 5 H_2O/ 0.004 HCl/ 0.14 CTAB. The dipping solution was aged for one week to allow for the silica network to adequately organize around the CTAB micelles. Supports were then dipped in the solution and dried in a laminar flow cabinet. These membranes were calcined at 500°C for 4 hr with heating and cooling rates of 1 °C min^{-1}.

Powders were obtained from each of the membrane synthesis methods. The powder from the hydrothermal synthesis was washed with H_2O and filtered to remove excess CTAB. The powder was then calcined under the same conditions as the hydrothermal membrane. The powder from

the dipped membrane was obtained by allowing the dipping solution to dry in the laminar flow cabinet. The dried dipping solution produced a clear film which was ground and then calcined under the same conditions as the dipped membrane. BET surface area measurements indicated that the powders made from the hydrothermal synthesis had a surface area 1500 m^2 g^{-1}, whereas the powder produced by the dipping process had a surface area of 880 m^2 g^{-1}. Such high surface areas are common for micellar templated mesoporous silica materials.

Figure 1 shows the pore size distribution for each of the powders computed by the Saito-Foley method using the N_2 adsorption isotherms. The hydrothermal synthesis powder has a unimodal pore size distribution centered at a pore diameter of 1.8 nm. The dip-solution powder has a unimodal pore size distribution centered at 2.0 nm. These results are also in agreement with previously published results on three dimensional cubic mesoporous silica materials.

Membrane thicknesses and compositions were determined by SEM and EDS. Figure 6 shows a SEM image of the hydrothermally fabricated SiO_2 membrane with a ~7 μm thick distinct top layer on top of the α-Al_2O_3 support with many defects visible on the micron scale. EDS analysis indicated that the SiO_2 also penetrates into the alumina support. The thin layer of SiO_2 deposited in the pores is likely responsible for the transport properties of this membrane (see Section 3.2). Figure 7 shows the dip-coated membrane which has a ~2μm thick SiO_2 layer. The SiO_2 particles which make up this layer appear to be much more uniform than those of the hydrothermal membrane, and is continuous and free of cracks
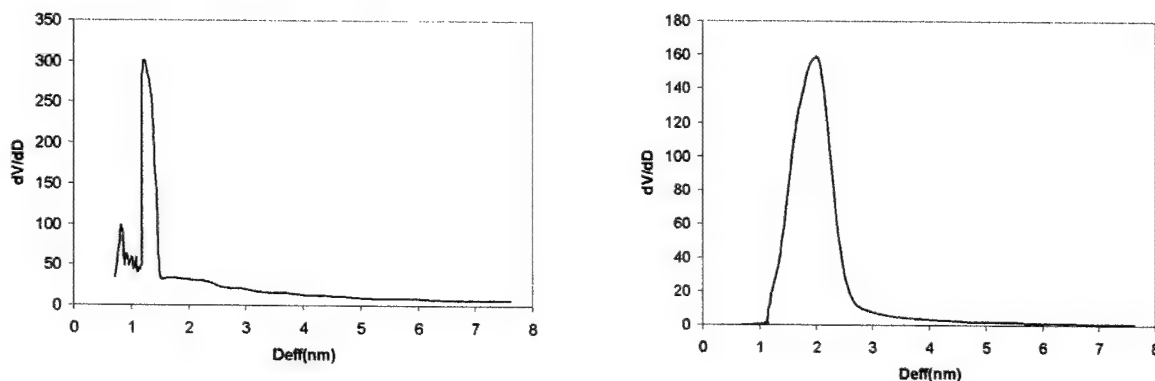
Figure 5 : Saito-Foley pore size distribution of three dimensional mesoporous silica powder fabricated by the hydrothermal process (left) and by the dip coating process (left).

Figure 6 : FE-SEM image of cross section of hydrothermal silica membrane
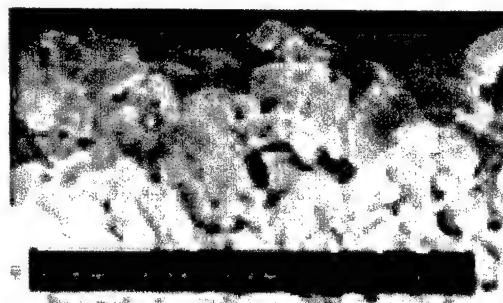
Figure 7 : FE-SEM image of cross section of dip coated silica membrane

3.2   Gas permeation through mesoporous membranes

The gas permeation for both types of membranes was measured before and after calcination. Both membranes were gas tight before calcinations indicating zero porosity, but after calcination they both exhibited large gas fluxes indicative of high surface area mesoporous membranes.

Membranes with pores in 2-20 nm range exhibit Knudsen diffusion as the dominating separation mechanism. In Knudsen diffusion the pore size of the membrane is on the same order as the mean free path of the gas molecules. In mesoporous membranes at pressures below 10 bar the permeation flux of a gas species, *i*, is completely determined by Knudsen flow. The flux of species *i* in this regime is given by:

$$J_i = \frac{\pi n r^2 D_k \Delta P}{RT\tau x} \qquad (1)$$

where n is the number of moles of gas and D_k is the Knudsen diffusion coefficient. The Knudsen diffusion coefficient is given by:

$$D_k = 0.66r\sqrt{\frac{8RT}{\pi M_W}} \qquad (2)$$

where M_w is the molecular weight of the species *i*. The ideal Knudsen separation factor of one gas over another, feed concentrations being equal, is then related only to the ratio of their molecular weights. Therefore the ideal Knudsen separation factor for species *i* over species *j* ($\alpha_{i/j}$) is given by:

$$\alpha_{i/j} = \sqrt{\frac{M_{Wj}}{M_{Wi}}} \qquad (3)$$

Knudsen diffusion also exhibits a weak temperature dependence of $T^{-1/2}$ as shown in equation (2) so we would also expect to see the permeance decrease slightly with temperature.

Membranes with larger pore sizes, like the macroporous supports used in this study, exhibit viscous flow. Viscous flow is not dependent on the size of the molecules. Therefore deviations from Knudsen diffusion separation will provide evidence that defects or cracks are present with the mesoporous membranes.

Figure 8 shows multigas separation results for Ar and N_2 through a MCM-48 membrane. The ideal Knudsen separation factor for N_2 over Ar is 1.19. However, the separation factor for the points taken over the temperature range of 25-200°C ranges between 1.2 and 1.35, which is slightly higher than Knudsen and in agreement with the pore size distribution measurements made on the powder. A slightly higher separation factor is expected because the lower limit of pure Knudsen diffusion is ~2 nm pores and the hydrothermal membrane pores are ~1.8 nm in diameter.

Figure 9 presents the same N_2/Ar multigas experiment for the 3-d cubic dipped membrane. The separation factor for N_2/Ar ranges from 1.1 to 1.15, which is slightly lower than expected for a Knudsen diffusion dominated process. This small deviation from ideal Knudsen diffusion is

likely due to a few microcracks in the membrane layer. Small defects and cracks often appear in thin films during the calcinations process. These defects can often be repaired by repeating the dipping process.
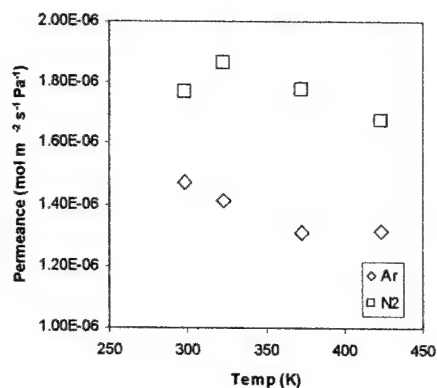

**Figure 8:** N_2/Ar separation data for multigas experiment using hydrothermal silica membrane.
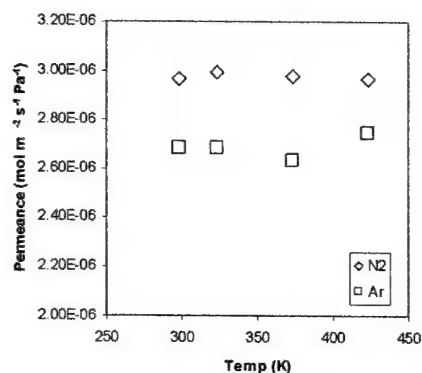
Figure 9: N_2/Ar separation data for multigas experiment using dip coated silica membrane.

Figure 10 shows gas permeation measurements for a variety of gases through the hydrothermal SiO_2 membrane. This experiment was performed by reading the pressure drop across the membrane with a differential Baratron gauge and setting the feed side mass flow controller such that the pressure drop was maintained at 760 torr. By plotting the gas flux through the membrane as a function of the molecular weight, a linear dependence on the inverse square of the molecular weight is obtained indicating that transport is dominated by Knudsen diffusion. Figure 11 presents similar gas permeation experiments performed on the dip-coated SiO_2 membrane. This membrane also exhibits a linear dependence versus the inverse square root of molecular weight. The fluxes for the dip-coated membrane are slightly higher than the MCM-48 as would be expected because of its slightly larger pore diameter.
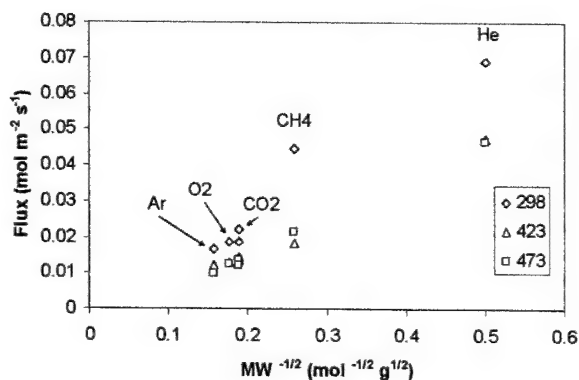
Figure 10: Single gas permeation data for several gases through hydrothermal silica membrane at 1 atm pressure drop.
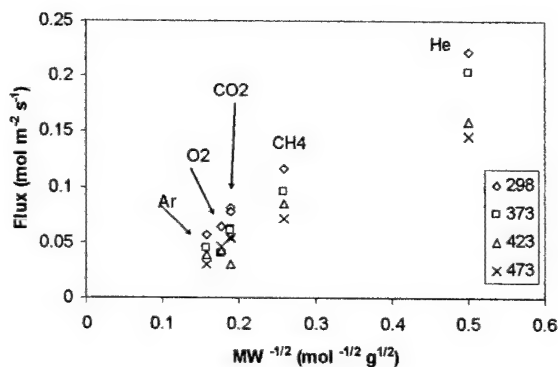
Figure 11: Single gas permeation data for several gases through dip coated silica membrane at 1 atm pressure drop.

In summary, the hydrothermally prepared membranes penetrate the support disk quite significantly, up to 50 μm. This type of membrane is potentially useful for modifying porous

thick film sensing materials like SnO_2 or WO_3. Penetration into the support ensures a fine distribution of the analyte among the conducting grains of the sensing material. Dip-coated silica membranes, however, are confined to the surface of the support. These membranes can be directly deposited on thin film SMO sensing elements. In both types of membranes, the pore size is in the mesoporous range, rendering gas separation to occur in the Knudsen flow regime. Modification of the pore size using atomic layer deposition can potentially refine this approach and enable molecular sieving.

3.3   Platinum/silica composite sensing films grown by chemical vapor deposition

Composite Pt/ SiO_2 films were made by CVD in a custom-built horizontal low pressure cold wall reactor. TEOS and $Pt(acac)_2$ precursors were used through a bubbler style vaporizer with argon carrier gas. $Pt(acac)_2$ was vaporized at 403K and TEOS was vaporized at 273K concurrently with different flow rates of O_2 and Ar. Depositions were carried out on r-cut sapphire substrates at 1.6 torr at substrate temperature ranging from 573-713K.

Several modifications to the reactor system were required to carry out *in situ* FTIR studies during the deposition process, particularly to allow the infrared beam to pass unobstructed through the reactor cell. This was accomplished using heated NaCl windows to avoid condensing unreacted precursor. A diagram of the reactor tube is shown in figure 12. The infrared beam passes straight through the reactor, and gas inlets and outlets are attached directly to the reactor tube.
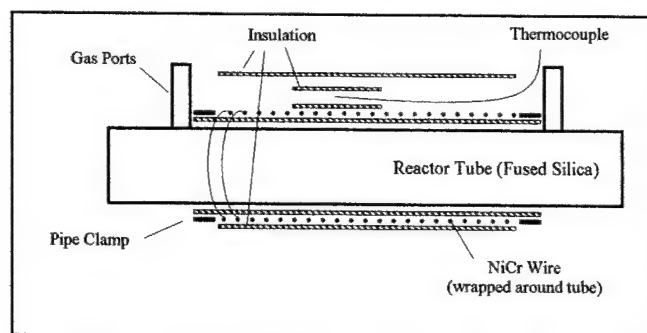
Figure 12a: CVD reactor design
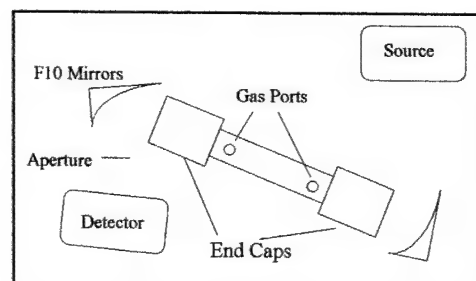
Figure 12b: Top view of CVD reactor showing integration with the FTIR spectrometer

Depositions were carried out at 673K varying the oxygen content of the atmosphere 0-70% which corresponded to growth rates from 1-4.4 nm/min. Films varied in reflectance, with low-carbon films being smooth and mirror-like and high-carbon films being rougher and unreflective. XRD analysis revealed a randomly oriented Pt crystalline phase and an amorphous silica phase. XPS analysis of the film stoichiometries (figure 13) indicated that the presence of O_2 has a marked affect on composition. A small amount of oxygen is required to have silicon incorporation into the film. Increasing the oxygen from 0% to 10% increases the amount of silicon from near zero to 14% of the film. The amount of carbon drops from 35% to 18% with just 10% oxygen, and drops slightly more with additional oxygen. The large amount of carbon suggests that the composite deposition process did not allow for the complete removal of precursor ligands. There was no deposition from TEOS alone at these conditions, neither on the r-cut sapphire substrates nor on a sapphire substrate pre-coated with platinum, even if the O_2 is increased to 95%. If the flow of $Pt(acac)_2$ is stopped, no further deposition occurs, consistent

with previous studies. When the deposition temperature was varied from 573K to 713K, silicon dioxide was incorporated into the film. The Si/Pt ratio goes through a maximum at 673K with a concurrent maximum in the growth rate.
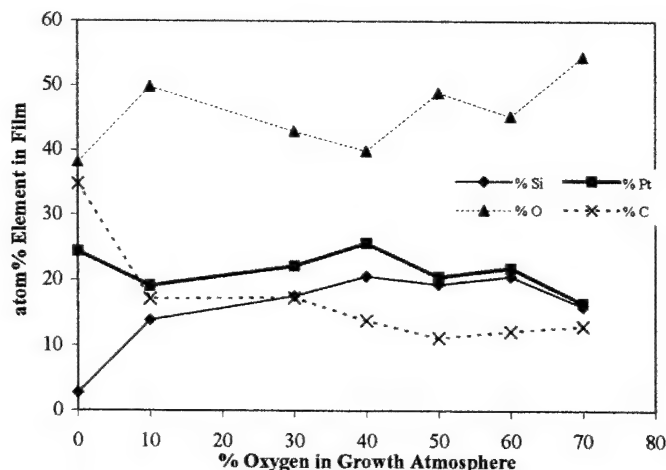
Figure 13 : Effect of Growth Atmosphere on Composite Film Composition

These Pt/SiO$_2$ composite films prepared by CVD have the potential to directly detect G-agents based on a highly selective two-step reaction sequence. The significant result achieved in this work was the ability to significantly lower the decomposition temperature of tetraethylorthosilicate by using the platinum acetyl acetonate precursor approach. Examination of the precursor interactions prior to reaching the substrate using an FTIR spectrophotometer configured around the CVD reactor revealed the mechanism for low temperature decomposition of TEOS in the presence of platinum acetyl acetonate.

4. Screened Decomposition Analysis

The adsorption and desorption of water, alcohols (including methanol, ethanol and isopropanol), and ethers (including dimethyl ether, DME, dimethoxymethane, DMM, and dimethyl methylphosphonate, DMMP) were studied using calibrated thermal desorption spectroscopy (CTDS) on the surfaces of epitaxially grown WO$_3$(001) films. The studies were conducted on oxidized and reduced WO$_3$(001) surfaces using x-ray photoelectron spectroscopy (XPS) and ultra-violet photoelectron spectroscopy (UPS) to monitor the W4f and valence band regions. The desorption spectra for molecular desorption of all the molecules mentioned above have very strong coverage dependence of desorption temperatures, and a significant shift of desorption temperature to low temperature with coverage, on both the reduced and oxidized WO$_3$(001) surfaces. Monte Carlo simulations show that this typical desorption shape can be characterized by first-order or pseudo-first-order desorption kinetics due to the surface heterogeneity and rapid diffusion. UPS shows that methanol adsorbs molecularly on the oxidized surface and dissociatively on the reduced surface, without other surface reactions detected.

A reaction controlled desorption of alkene was identified from dehydration of ethanol and isopropanol on both the reduced and oxidized surfaces in which C-O bond scission was verified as the rate-limiting step for ethanol and for isopropanol. However, the selectivities of both surfaces toward dehydration of alcohol to alkene do not have a significant difference. A

mechanism involving surface competition reaction kinetics and diffusion control can be used to explain the selectivity toward alkene, which is in marked contrast with the defect controlled model on the TiO$_2$(110) surface. Methanol was observed from adsorption of DMM on both surfaces and no reaction product was detected for DME adsorption. DMMP decomposed on both the reduced and oxidized surfaces through loss of a methoxy group by breaking the P-OCH$_3$ bond; however, methanol and DME were detected on the oxidized surface and only DME was observed on the reduced surface. Phosphorus was detected in XPS on both surfaces after DMMP desorption experiments indicating a poisoning effect on the oxidized surface. A new C1s XPS band, observed after DMMP exposure on both surfaces, is assigned to P-CH$_3$ species after decomposition of the DMMP molecule. These detailed kinetic signatures associated with decomposition reactions are significant for developing WO$_3$ sensor elements selective to organophosphate species.

4.1 Methanol interaction with WO$_3$ surfaces

We prepared two types of WO$_3$(001) surfaces, referred to as oxidized and reduced, which are characterized by strong Lewis acid sites in which the terminal oxygen is removed, leading to tungsten cations, in a formally 5+ or 4+ oxidation state. On the oxidized surface, UPS shows that methanol bonds molecularly to Lewis sites, while on the reduced surface, stronger Brønsted base sites lead to dissociative adsorption.

The coverage dependent desorption of methanol shows strong shifts to lower temperature as shown in Figure 14, similar to behavior of water and other alcohols on oxide surfaces. Monte Carlo simulations allow the relative importance of diffusion and desorption to be assessed from coverage dependent spectra. Qualitatively different behavior is also found for the effects of a heterogeneous surface and intermolecular interactions, for both the cases of slow and rapid diffusion. On WO$_3$, diffusion of molecular methanol is relatively rapid. The structural constraints of the large tungsten-oxygen-tungsten cation distances appear to prevent significant hydrogen bonding between adsorbed methanol molecules. Thus, the coverage dependence of the desorption spectra is attributed to the heterogeneity of the adsorbate-surface interaction.

4.2 Aliphatic alcohol reaction on WO$_3$ surfaces

Reactions of alcohols on the reduced and oxidized WO$_3$(001) surfaces were conducted at very low coverages. Alcohols were removed from the surfaces through two channels: low temperature desorption of alcohol with desorption spectra that indicate a broad distribution of adsorption site energies and diffusion rates that are sufficiently rapid for the alcohol to find and desorb from the most strongly bound sites; and dehydration to form an alkene, which desorbs at higher temperature together with desorption of water. Desorption of the alkene is a reaction controlled process, and the rate-limiting step for dehydration of ethanol and isopropanol, is C-O bond scission. The reduced and oxidized WO$_3$(001) surfaces do not have significant differences in their selectivity toward dehydration of the alcohols to alkenes. The coverage dependence of the selectivity can be attributed to the role of diffusion and reaction kinetics under the low

coverage conditions, which contrasts with the dehydration of alcohols on the TiO$_2$(110)[35] and TiO$_2$(001)[36] surfaces.
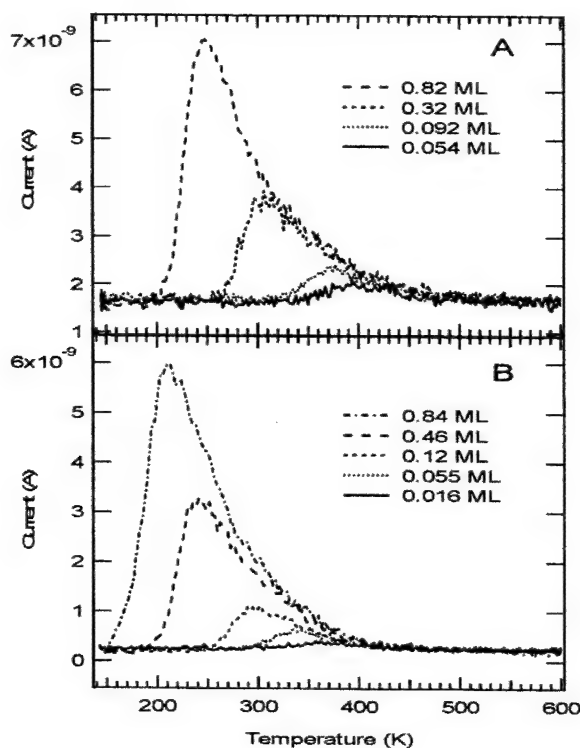
Figure 14 : Thermal desorption spectra of methanol (31 amu signal) on A) reduced WO$_3$(001) surface; and B) oxidized WO$_3$(001) surface. Dosing of methanol was performed at 140 K through a microarray doser, and the temperature ramp rate was 4 K/sec.

4.3 Ether interaction with WO$_3$ surfaces

Adsorption and desorption experiments involving dimethyl ether (DME) and dimethoxymethane (DMM) were performed on the reduced and oxidized WO$_3$(001) surfaces with calibrated thermal desorption spectroscopy. DME molecularly adsorbs and desorbs on both the reduced and oxidized surfaces without decomposition products detected. For DMM adsorption (Figure 15), two molecular desorption peaks were observed and a reaction controlled desorption of methanol, formed from decomposition of DMM, was identified. Based on the comparison of desorption peak temperatures of ethers and alcohols, the low temperature peak is attributed to DMM interacting with a single tungsten cation through oxygen lone pair electrons. The higher temperature peak that appears only on the reduced surface is assigned to DMM interacting with two tungsten cations through both ether oxygens, perhaps in regions associated with

---

[35] Gamble, L.; Jung, L. S.; Campbell, C. T. *Surf. Sci.* **1996**, *348*, 1-16.

[36] Kim, K. S.; Barteau, M. A. *J. Molecular catalysis* **1990**, *63*, 103-117.

crystallographic shear structure domains. The possible role of DMM as a probe molecule in studying closely spaced metal cation sites, on the WO₃ surface and other oxides, is noted.
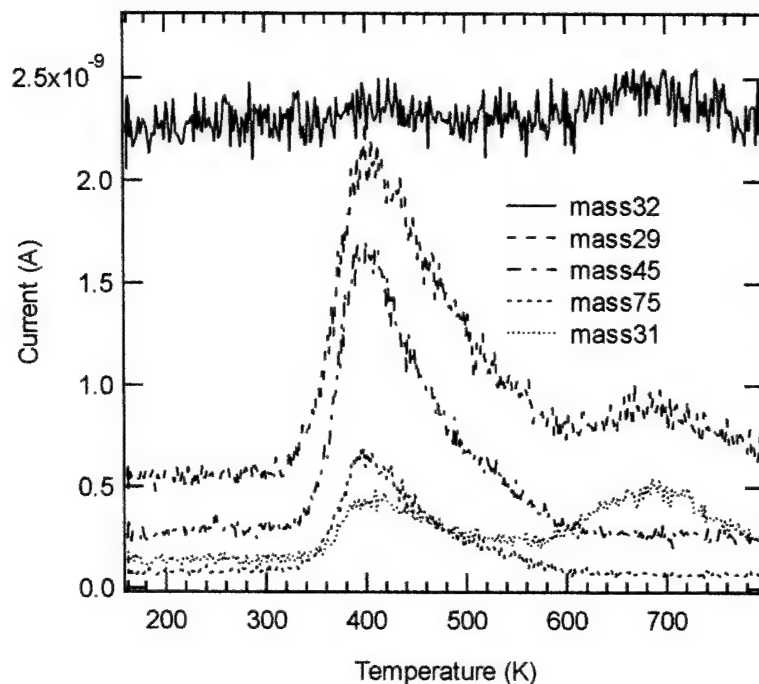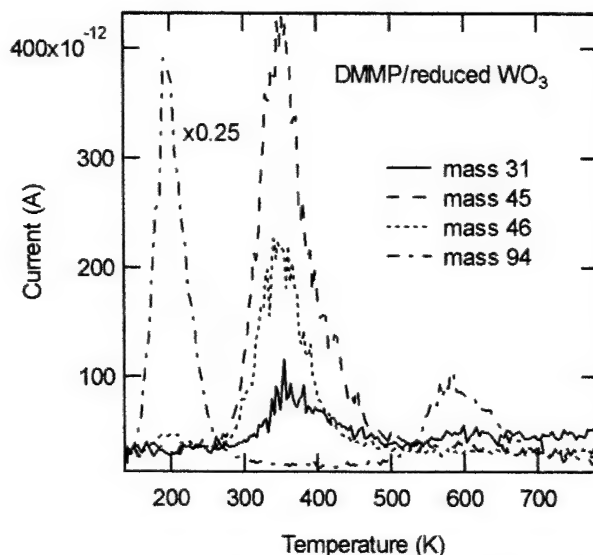

Figure 15 : A representative desorption spectrum of dimethoxymethane (DMM) on the reduced WO₃(001) surface. The desorption peak at 400 K is attributed to molecular desorption of DMM, while the peak at 690 K is assigned to desorption of methanol, produced from decomposition of DMM, based on their fragmentation patterns.

4.4 Organophosphonate interaction with WO₃ surfaces

Adsorption and decomposition of dimethyl methylphosphonate (DMMP) was carried out on the reduced and oxidized WO₃(001) surfaces using calibrated thermal desorption spectroscopy (CTDS). Multilayer desorption of DMMP was not detected on either surface, while the monolayer desorption, attributed to molecularly adsorbed DMMP species, was observed around 600 K. The desorption temperature of chemisorbed DMMP appears to be consistent with the dependence on molecular weight of the desorption temperatures of alcohols and ethers studied on these surfaces. On the oxidized WO₃(001) surface, dimethyl ether and methanol were produced during decomposition of DMMP. However, on the reduced surface, dimethyl ether was observed but no methanol was observed (Figure 16). The desorption of DMMP decomposition products shows that DMMP decomposes below 450 K on the WO₃(001) surfaces.

We associate the lower temperature decomposition of DMMP to dimethyl ether to adsorption on more strongly bound sites, which have been identified in the study of dimethoxymethane adsorption on the reduced surface. These surface sites may be related to emergence of crystallographic shear (CS) planes at the surface, in which the spacing between Lewis acid sites

is expected to be reduced compared to the majority 5-fold W^{6+} sites. We suggest that adsorption occurs through two Lewis acid-base interactions between adsorbate and adsorbent.

Figure 16: A representative set of desorption spectra following adsorption of DMMP on the reduced $WO_3(001)$ surface. DMMP molecular desorption was observed at 580 K and desorption of DME, produced from decomposition of DMMP, was observed at 350 K; the large desorption at mass 94 at 200 K is probably due to contaminant methyl bromide.

Dimethyl ether and methanol, produced from decomposition of DMMP, desorbs at lower temperatures compared to the desorption temperature following adsorption of dimethyl ether or methanol, respectively. Given the behavior of methanol on both the reduced and oxidized surfaces, on which dimethyl ether was not detected, even on the reduced surface where methanol adsorbs dissociatively, production of dimethyl ether most likely occurs through an intramolecular coupling reaction. The production of methanol was determined by the availability of surface hydroxyls during the decomposition process. $P-CH_3$ species are identified in XPS on both the reduced surface and oxidized surface after decomposition of DMMP. Accumulation of phosphorus results in poisoning of the surface reaction. The surface processes of DMMP on the $WO_3(001)$ surfaces suggested in this study are consistent with our infrared observations in the study of DMMP adsorption on WO_3 powders (Section 2); however, our mechanism differs from the widely accepted decomposition mechanism on the Al_2O_3 surface and some other oxide surfaces. Thermal desorption studies on the powder materials and vibrational studies on our thin film surfaces are needed to resolve the difference in interpretation.

5. SMO Element Optimization

Our general approach has been to synthesize thin (thickness between 20 nm and 250 nm) heteroepitaxial tungsten oxide films on the sapphire single crystal substrates using magnetron sputtering. To order to influence selectivity, the tungsten oxide films were deposited in either pure form or containing monolayer amounts of metal (e.g. Au, Pt) or metal oxide (e.g. TiO_2, SnO_2, CuO) surface catalysts. A key result that we found was that deposition of well-defined

epitaxial microstructures leads to improved sensor stability and reproducibility. Experiments were also carried out to explore the epitaxy of WO_3 on BaF_2/Si substrates supplied by researchers from NSWC-Dahlgren, which is a step towards integrating the SMO sensors and associated Si-based electronics directly on a Si wafer.

5.1 WO_3 film epitaxy on sapphire substrates

On the r-cut sapphire substrates, the WO_3 film structure depends on the growth temperature. Films grown between room temperature and 200°C yield diffuse RHEED and XRD patterns indicating the films have an amorphous or very small nanocrystalline structure. At the other extreme, above 800°C, the WO_3 evaporates from the sapphire surface and hence there is no sticking during attempted growth. In the intermediate temperature range, two types of heteroepitaxial structure are formed with the highest quality diffraction patterns occurring at 450°C and 650°C. Based on the symmetry and lateral spacings of the RHEED patterns, these phases can be indexed to the tetragonal WO_3 phase oriented with (001) parallel to the (01•2) sapphire substrate at 450°C and the monoclinic WO_3 phase oriented with (001) parallel to the (01•2) sapphire substrate at 650°C. On the c-cut sapphire substrates, the WO_3 film diffraction features are sharpest after 700°C growth, and can be indexed to a metastable hexagonal WO_3 phase. Growth at lower temperatures results in diffuse complicated RHEED patterns indicating poor epitaxy and complex structures.

Based on RHEED and XRD data, we conclude that tetragonal, monoclinic, or hexagonal WO_3 phases can grow heteroepitaxially on sapphire. However, these films are not single crystalline but are highly textured and better described as having a 'polycrystalline epitaxial structure'. Experiments were performed to monitor the reproducibility of the film quality. To obtain the best structural quality, the deposition rate must be limited to below 0.02 nm/s. Figure 17 shows XRD θ–2θ scans from multiple depositions of 250 nm thick films using the exact same deposition parameters. The tetragonal WO_3 films show a large variability in terms of peak width, exact peak position, and magnitude of the small monoclinic component (Fig.17a) suggesting variability in the amount of strain and crystalline quality. However, the monoclinic WO_3 films exhibit very reproducible XRD spectra (Fig.17b). These results on film reproducibility have large implications for quality control in sensor device fabrication.

The morphologies of the film growth surfaces were examined using *in situ* STM imaging. Figure 18 shows 200 nm x 200 nm images acquired from each of the WO_3 film types at a film thickness of 50 nm; the surface rms roughness was less than 2 nm in each case. The tetragonal phase (Fig.18a) consists of a granular morphology with each grain being ~30 nm in diameter, and the growth surface does not exhibit any features corresponding to the rectangular symmetry of the r-cut sapphire substrate. Considering that the diffraction data indicated that all of the grains nominally have the same orientation, the dark boundaries probably arise from antiphase and low angle boundaries between each of the crystallites. The surface of the monoclinic phase (Fig.18b) displays a step-terrace morphology, which suggests that film growth proceeds by a 3-dimensional growth mechanism with adatom attachment occurring at the terrace edges. The edges of terraces have preferred directions indicative of low energy step orientations. The hexagonal phase (Fig.18c) also exhibits a granular structure with several grains being elongated

in directions consistent with the hexagonal symmetry of the c-cut sapphire substrate. These WO_3 film morphologies play a big role in stabilization of dispersed catalytic nanoparticles.
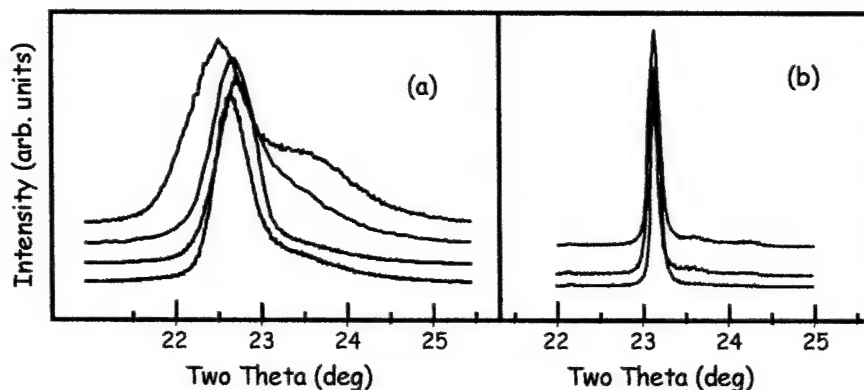
Figure 17: X-ray diffraction scans from (a) tetragonal and (b) monoclinic WO3 films following multiple depositions of each film type to monitor reproducibility of crystalline quality.
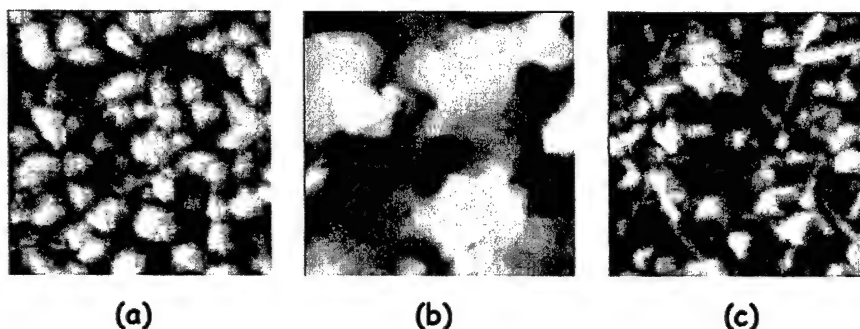

Figure 18: 200 nm x 200 nm STM images from growth surfaces of 50 nm thick WO_3 films. (a) tetragonal phase, rms roughness = 1.4 nm (b) monoclinic phase, rms roughness = 1.9 nm (c) hexagonal phase, rms roughness = 1.3 nm.

Measurements of film conductivity and mobility versus temperature using our Hall effect characterization system indicate that the charge transport mechanisms are also dependent on the crystallographic phase and microstructure of the WO_3 films. Whether the conduction is dominated by charge motion within the crystallites or across defect boundaries can dictate different sensor operating regimes and gas response. The number of charge carriers depends critically on the exact WO_{3-x} stoichiometry since they are dictated by the oxygen vacancy population. However, the mobility of the carriers is influenced by the film microstructure including crystal defects and low-angle grain boundaries. The conductivity, the quantity measured in a chemiresistive sensor, depends both on the carrier concentration and the mobility. To characterize the effect of microstructure on charge transport, conductivity measurements were carried out on each of the epitaxial WO_3 film types.

Following growth, the WO_3 films were transferred into the conductivity apparatus, annealed in UHV at 400°C for 5 hours to establish a well-defined stoichiometry and oxygen vacancy

population, and then the conductivity was measured as a function of temperature as shown in Figure 19. The conduction in WO_3 is believed to occur via a polaron mechanism, which involves hopping of charge between distorted lattice sites. The slope of the log conductivity versus inverse temperature plot is related to the activation energies for carrier ionization and hopping. All three film types have an activation energy of ~0.2 eV, but the conductivity of the monoclinic WO_3 film is an order of magnitude lower than the tetragonal and hexagonal WO_3 film. This result is significant since lower baseline conductivity leads to larger sensor sensitivity from carrier generation caused by surface oxidation/reduction reactions. The conductivity behavior is very reversible with repeated thermal cycling suggesting that the well-defined heteroepitaxial film structures are stable over time.
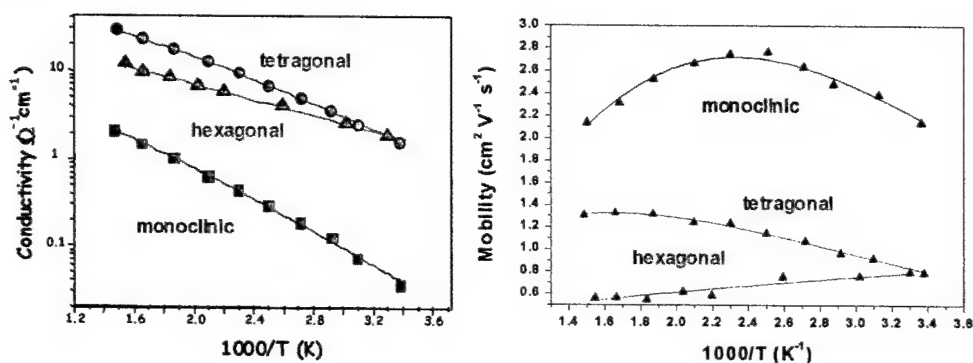
Figure 19: (a) Conductivity and (b) Hall mobility measurements versus temperature for three different thin film phases of WO_3.

5.2 WO_3 growth on BaF_2/Si substrates

In this phase of the work, Si (100) substrates covered by a high quality (111) oriented BaF_2 buffer layer were received from Naval Surface Warfare Center – Dahlgren. We characterized these substrates and found that the 30 nm thick BaF_2 layers, grown by very low rate MBE, consist of four equivalent crystalline domains oriented about the BaF_2 <111> axis, and these domains provide a good template for growth of heteroepitaxial WO_3 domains.

A significant finding was that magnetron sputter deposition of WO_3 (using the process followed on sapphire substrates) did not work. The reason for this is that the high energy electron and ion bombardment during sputtering causes extensive damage and loss of fluorine in the BaF_2 layer. However, we found a very successful way to achieve high quality WO_3 films by using electron cyclotron resonance (ECR) oxygen plasma-assisted electron beam evaporation of a WO_3 source over the temperature range of 25 – 600°C. At an optimal deposition temperature of 450°C, the monoclinic WO_3 phase was produced and the film consisted of coexisting (002), (020), and (200) in-plane orientations with respect to the $BaF_2(111)/Si(100)$ substrate. During growth, an interfacial barium tungstate ($BaWO_4$) reaction product formed at the WO_3-BaF_2 interface. The {112} planes of this $BaWO_4$ layer also have a multi-domained epitaxial orientation with respect to the BaF_2 buffer layer. Post-deposition annealing experiments in air for 24 hours at 400°C indicated that this WO_3-$BaWO_4$-BaF_2-Si architecture remains stable, indicating that this substrate is a potential alternative to sapphire for future SMO sensor development.

5.3 Dispersed copper oxide nanoparticles on epitaxial WO₃ films

We prepared sensor films by deposition of Cu_2O at room temperature on the epitaxial WO_3 films on sapphire substrates. Initially the Cu_2O is amorphous but, after annealing in air, becomes crystalline and converts partly to CuO in the surface region. XPS and XRD measurement are consistent with changes in morphology from a Cu_2O overlayer to 3-dimensional islands for nominal coverages in the 2-3 nm regime. Upon exposure of the sensors to DMMP, for films of intermediate Cu_2O coverage, the islands re-disperse and the extent of phosphorus uptake correlates with the recovery of the Cu/W ratio.

Figure 20a shows the Cu2p to W4f peak XPS ratio for during the stages of sensor preparation and processing. After deposition, the sensors were mounted on a carrier for XPS analysis and reintroduced to the vacuum system. Initially, the Cu/W ratio was consistent with the Cu_2O film coverage. The copper signal decreased after the sensors were calibrated in air, which could be due to aggregation, diffusion into the WO_3 film, or ternary phase formation. The Cu2p/W4f ratio increased after DMMP exposure and, in fact, was larger than when the sensor was "new", for the 3 and 15Å thicknesses. This suggests either surface segregation or re-dispersion of particles if aggregation occurred during the annealing step. The maximum effect was found for the 15Å nominal coverage and 300-400 °C temperature range.
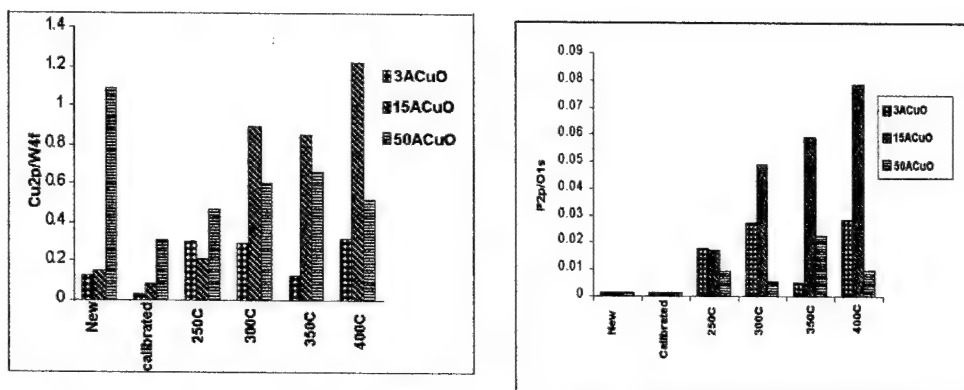
Figure 20: (a) Cu2p/W4f and (b) P2p/O1s XPS peak area ratios after deposition ("new"), annealing and calibration ("calibrated"), and exposure to methanol, DMMP, and methanol at 250, 300, 350 or 400 °C.

The P2p/O1s peak area ratios are plotted in Figure 20b. The phosphorus coverage was negligible after initial fabrication and after calibration to 400 °C in air, suggesting that background levels of volatile phosphonates in the laboratory environment are low. After DMMP exposure, the phosphorus uptake was greatest for the intermediate Cu_2O film thickness of 15Å and at an exposure temperature in the 300 to 400 °C range. This correlates with the recovery in the Cu2p/W4f ratio (Figure 20a). The dramatic morphology changes after DMMP exposure has important ramifications for SMO sensor operation. This behavior indicates that development of a dosiometric sensor can be pursued that responds to the phosphorus poisoning.

6. Sensor Response Signature Analysis

### 6.1 Quantifying gas sensor and delivery system response time

We examined how properties of our sensor gas delivery test system can introduce errors into measurements of sensitivity, reproducibility and response time of SMO sensors. This characterization of the performance was carried out using a gas chromatograph/quadrupole mass spectrometer (GC/MS) and custom designed gas sampling system. The important result is that the accuracy of parameters extracted from the sensor response incorporates both the delivery system characteristics and surface reaction kinetics on SMO sensors. Our analysis showed that effects of the test system on response time are significant, particularly at lower concentrations and for less volatile compounds. Sensor to sensor reproducibility is critically dependent upon sensor RTD temperature calibration, while the variation in sensor response from pulse to pulse is controlled by the gas delivery system. These critical issues are often not taken into account in sensor response measurements quoted in the literature. We published a comprehensive report of these issues associated with gas delivery system response and sensor kinetics in *Sensors and Actuators*.[37]

6.2 Differentiating between organophosphonates and alcohols

We concentrated on the analysis of sensor response kinetics for five different types of sensors. For the five differently modified WO_3 sensor types, quantification of the conductivity change during exposure to a particular gas gives responses that differ by several orders of magnitude (Figure 21). We have quantified the temperature-dependence of these responses to different gases, e.g. DMMP (simulant) vs. methanol (interferent), and for each sensor type the temperature dependence to alcohols and organophosphonates was compared (Figure 22). We found significant differences for WO_3 modified with CuO and TiO_2, showing that the slope is a concentration-independent feature, which can be used to distinguish between these two classes of compounds (Figure 23). Notice that the alcohols (red symbols) have stronger temperature dependence than the phosphonates (blue symbols) on CuO, while the pattern is reversed on TiO_2 modified and pure WO_3. This suggests that the rate limiting step in the kinetics of DMMP decomposition is different from that for methanol on these surfaces. By contrast, pure WO_3 films show a similar temperature dependent response. Concentration dependent measurements (Figure 24) also differentiate between these gases, but the signal to noise ratio is not as large in the data obtained to date. Nevertheless, both methods offer means of improving selectivity.

Previous measurements showed that sensor sensitivity exceeded the capabilities of the delivery system to deliver pulses of gas at concentrations in the 10 ppb range for DMMP (simulant). Therefore, improvements were made to the gas sensor testing system and procedures used to prepare gas mixtures for sensor testing to reproducibly deliver simulants at the 10 ppb level. An air purification system was installed to reduce total hydrocarbons in the carrier gas (used for the blank) to below 50 ppb, which is significantly lower than the best (several ppm) quality synthetic air which is commercially available. A comparison of the hydrocarbon content of the previous
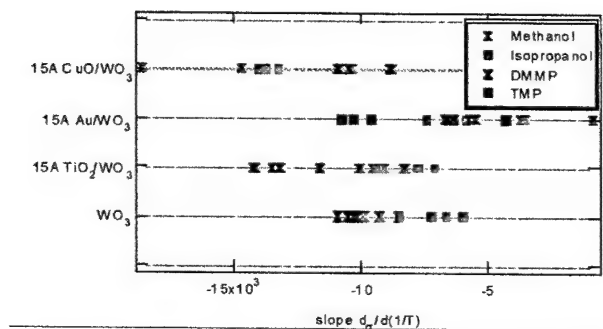
---

[37] R. S. Pilling, G. Bernhardt, C. S. Kim, J. Duncan, C. B. H. Crothers, D. Kleinschmidt, D. J. Frankel, R.J. Lad, and B. G. Frederick, *Quantifying Gas Sensor and Delivery System Response Time using GC/MS*, Sensors & Actuators, in press (2003).
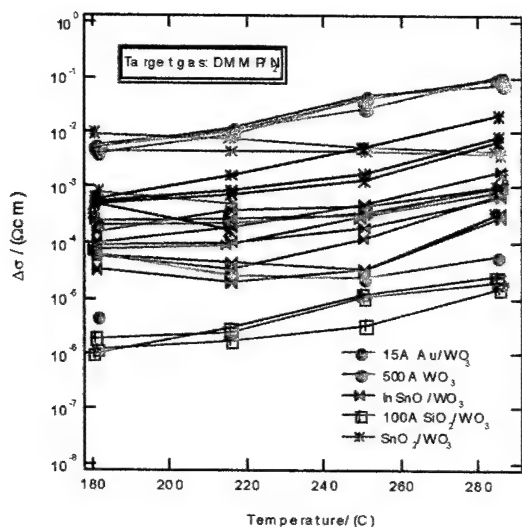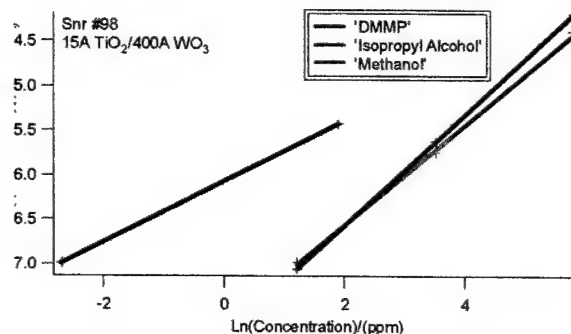
Figure 21: Response to DMMP for five types of modified WO₃ sensors.
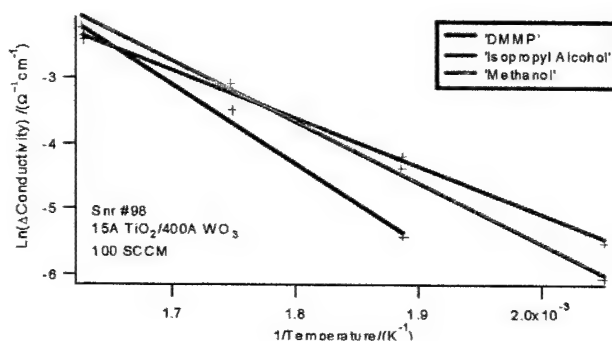
Figure 22: Temperature dependent response to alcohols and DMMP

Figure 23: Temperature dependent slope as a means of identifying alcohols and organophosphonates.


**Figure 24:** Concentration-dependent measurements.

carrier gas (Grade 2.0 Air) to that produced by the Zero Air Generator is illustrated in Figure 25. When the Grade 2.0 air is delivered to the sensors as the "target" gas (red curve), the resistance drops significantly, as expected if the generated air has <50 ppb total hydrocarbon content. When the generated air is delivered as the "target gas", the conductivity change reverses (black curve). Carrier gas and gas mixtures are now derived from this source and GC/MS measurements confirm the improved quality of the gases.

Heaters were added to the sensor testing system and the response time was measured with the GC/MS at elevated temperatures. Improvements in the step response time for methanol, isopropanol and DMMP were observed, particularly during recovery after exposure. For some sensors, the sensor response-time was limited by the 9-second time constant of the delivery system. Figure 26 compares the change in conductivity of a WO₃ sensor during exposure to a high concentration of methanol to measurements (red curve) of the methanol concentration with
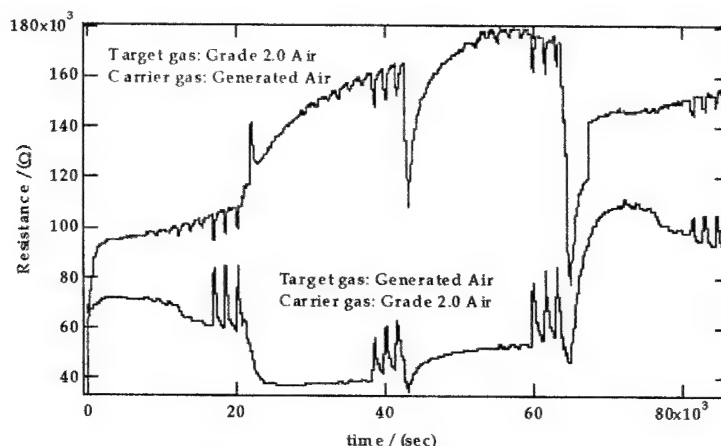
Figure 25. Comparison of sensor response when using bottled carrier gas (Grade 2.0 Air) versus a Zero Air Generator shows the effect of residual hydrocarbons in the bottled gas.
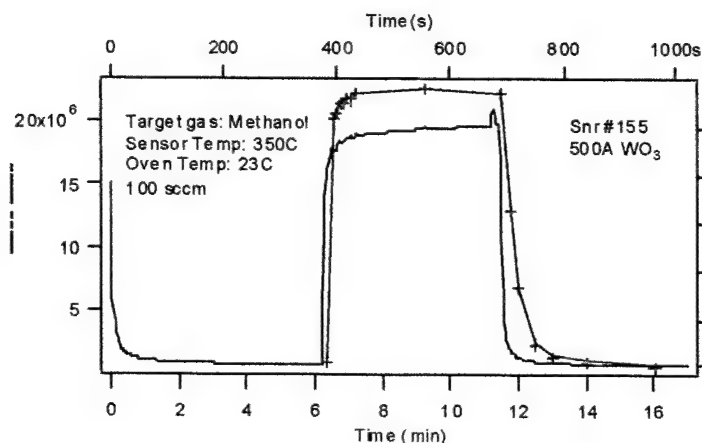
Figure 26. Conductivity change of WO_3 sensor during high exposure to methanol (red curve) compared to the response of the gas delivery system as measured by the GC/MS.

the GC/MS gas sampling system. The time constant of the delivery system during recovery (Figure 27) improves with increasing temperature, but is significantly larger for organo-phosphonates than for the more volatile alcohols. This implies that the sensor response time is significantly faster than the delivery system response, and development of sensors with response times below 10s is possible, but will require further improvements to the fluid-flow characteristics of the sensor testing system.
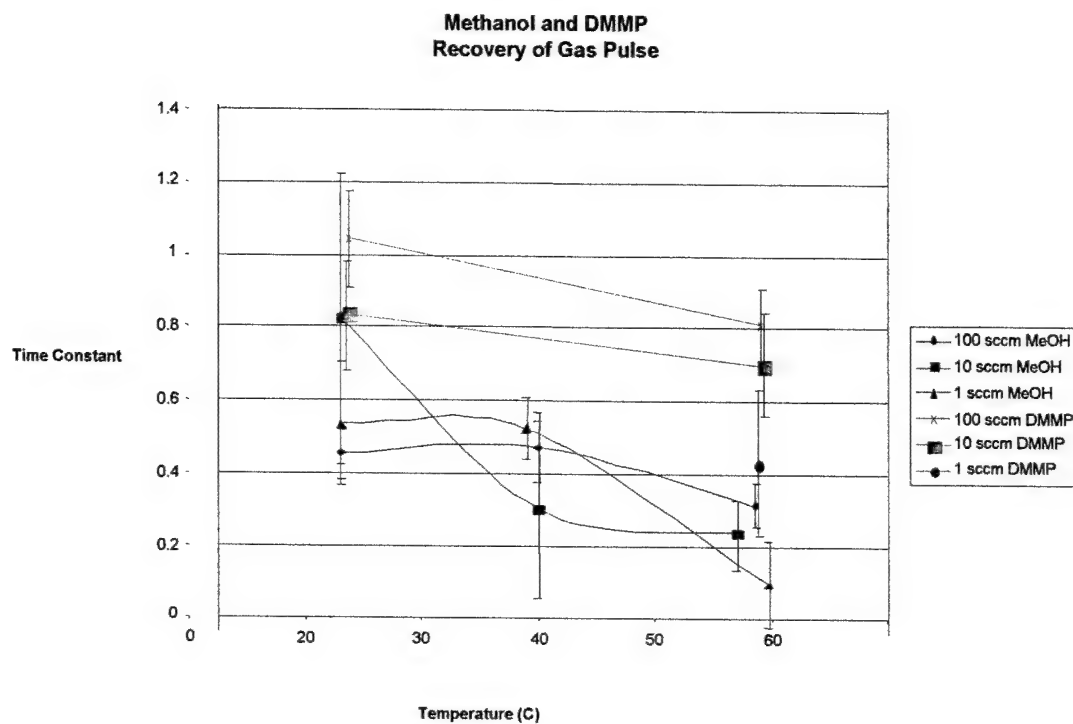
Figure 27. Time constant of methanol and DMMP recovery in the gas delivery system, measured by GC/MS as a function of temperature of the gas lines.

7. Research Publications, Presentations, and Patents

PUBLICATIONS:

1. B. J. Ninness, D.W. Bousfield and C. P. Tripp, *An In Situ Infrared Technique for Studying Adsorption onto Particulate Silica Surfaces from Aqueous Solutions,* Appl. Spectrosc. 55, 655 (2001)

2. S. M. Kanan and C.P. Tripp, *An Infrared study of Adsorbed Organophosphonates on Silica: A Prefiltering Strategy for the Detection of Nerve Agents on Metal Oxide Sensors,* Langmuir 17, 2213 (2001)

3. C. S. Kim, R. J. Lad and C. P. Tripp, *Interaction of Organophosphorous Compounds with TiO_2 and WO_3 Surfaces Probed by Vibrational Spectroscopy,* Sensors and Actuators B 76, 442 (2001)

4. S.C. Moulzolf, L.J. LeGore, and R.J. Lad, *Heteroepitaxial Growth of Tungsten Oxide Films on Sapphire for Chemical Gas Sensors,* Thin Solid Films 400, 56 (2001).

5. H. Li and C. P. Tripp, *Spectroscopic Identification of the Structure and Dynamics of Adsorbed Surfactants on Charged Metal Oxide Surfaces* Langmuir 18 , 9441 (2002)

6. S. M. Kanan, Z. Lu, and C. P. Tripp, *A Comparative Study of the Adsorption of Chloro and Non-Chloro Containing Organophosphonates on WO_3,* J. Phys. Chem. B 106, 9576 (2002)

7. S. M. Kanan, W. T.Y. Tze, and C. P. Tripp, *A Method to Double the Surface Concentration and Control the Orientation of Adsorbed (3-aminopropyl) dimethylethoxysilane on Silica Powders and Glass Slides* Langmuir 18, 6623 (2002)

8. Z. Lu, S. M. Kanan and C.P. Tripp, *Synthesis of Nano-sized Monoclinic WO_3 Particles Using Chelating Ligands and Emulsion Based Methods,* Chem. Mater. 12, 983 (2002)

9. B. J. Ninness, D.W. Bousfield and C. P. Tripp, *The Importance of Adsorbed Cationic Surfactant Structure in Dictating the Subsequent Interaction of Anionic Surfactacts and Polyelectrolytes with Pigment Surfaces,* Colloids and Surfaces A. 203, 21 (2002)

10. S. M. Kanan, Z. Lu, J. K. Cox, G. Bernhardt and C.P. Tripp, *Identification of Surface Sites on Monoclinic WO_3 powders by Infrared Spectroscopy,* Langmuir 18, 1707 (2002)

11. S. M. Kanan and C.P. Tripp, *Prefiltering Strategies for Metal Oxide Based Sensors: Use of Chemical Displacers to Selectively Cleave Adsorbed Organophosphonates from Silica ,* Langmuir 18, 722 (2002)

12. L.J. LeGore, R. J. Lad, J. F. Vetelino, B. G. Frederick, *Defects and Morphology of Tungsten Trioxide Thin Films,* Thin Solid Films 406 79 (2002).

13. S.C. Moulzolf, D.J. Frankel, and R.J. Lad, *In-situ 4-point Conductivity and Hall Effect Apparatus for Vacuum and Controlled Atmosphere Measurements of Thin Film Materials,* Reviews of Scientific Instruments 73, 2325 (2002).

14. R.J. Lad, *Heteroepitaxy of Tungsten Oxide Films on Sapphire and Silicon for Chemiresistive Sensor Applications*, First IEEE Sensors International Symp. Proc. 44.1 (2002).

15. Tyler P. Martin, *Platinum Silica Thin Films by Chemical Vapor Deposition*, M.S. Thesis, Chemical Engineering, University of Maine (2002).

16. B. J. Ninness, D.W. Bousfield and C. P. Tripp, *Formation of a Thin TiO₂ Layer on the Surfaces of Silica and Kaolin Pigments Through Atomic Layer Deposition* Colloids and Surfaces 203, 21 (2003)

17. S. Ma, F.G. Amar and B.G. Frederick, *Surface Heterogeneity and Diffusion in the Desorption of Methanol from WO₃ (001) Surfaces*, J. Phys. Chem. A 107 1413 (2003).

18. R. S. Pilling, G. Bernhardt, C. S. Kim, J. Duncan, C. B. H. Crothers, D. Kleinschmidt, D. J. Frankel, R.J. Lad, and B. G. Frederick, *Quantifying Gas Sensor and Delivery System Response Time using GC/MS*, Sensors & Actuators, in press (2003).

19. A. El Madi, B. Meulendyk, R. S. Pilling, G. Bernhardt, R. J. Lad, and B. G. Frederick, *Phase and Morphology in Mixed CuO-WO₃ Films for Chemical Sensing*, Mat. Res. Soc. Proc. 751, in press (2003).

20. B.A. McCool, N. Hill and W.J. DeSisto, *Synthesis and Characterization of 3-d Cubic Mesoporous Silica Membranes via Dip-Coating and Hydrothermal Deposition Techniques* (submitted)

21. S. Ma and B.G. Frederick, *Reactions of Aliphatic Alcohols on WO₃(001) Surfaces*, J. Phys. Chem. A (submitted).

22. S. Ma and B.G. Frederick, *Surface Reactions of Ethers on WO₃(001) Surfaces*, J. Phys. Chem. A (submitted).

23. S. Ma and B.G. Frederick, *Effect of Surface Reduction on Decomposition of Dimethyl Methylphosphonate on Tungsten Trioxide Surfaces*, J. Phys. Chem. A (submitted).

24. L.D. Doucette, F. Santiago, S.L. Moran, R.J. Lad, *Hetereopitaxial Growth of Tungsten Oxide Films on Silicon (100) using a BaF₂ Buffer Layer*, J. Materials Research (submitted).

PRESENTATIONS:

1. R.J. Lad, *Ultra-thin Tungsten Oxide Based Films for Chemical Sensors*, Spring 2001 Meeting of the European Materials Research Society, Strasbourg, France, June 7, 2001 (invited).

2. B.J. Ninness, D.W. Bousfield and C.P. Tripp, *An In situ Spectroscopic Method for the Detection of the Attachment Chemistry of Biomolecules to Silanized Surfaces*, American Colloid and Surface Science Conference, Pittsburgh, June 10-13, 2001.

3. S.C. Moulzolf and R.J. Lad, *Electronic Transport Mechanisms in WO₃-Based Ultra-thin Film Chemiresistive Sensors*, The 11th International Conference on Solid-State Sensors and Actuators, Transducers '01, Eurosensors XV, Munich, Germany, June 14, 2001.

4. S. Ma, R.L. Jackson and B.G. Frederick, *Effect of Surface Reduction on Decomposition of Dimethyl Methyl Phosphonate on Tungsten Trioxide Surfaces*, 30th American Chemical Society Northeast Regional Meeting, Durham NH, June 24-27, 2001.

5. R. S. Pilling, C. S. Kim, S. C. Moulzolf, G. Bernhardt, B. G. Frederick, *Selectivity toward Organophosphorous Compounds in SMO Chemiresistive Sensors*, 30th American Chemical Society Northeast Regional Meeting, Durham NH, June 24-27, 2001.

6. C. P. Tripp, *Infrared Spectroscopic Studies of Silica Conducted in the Gas Phase, Aqueous and Non Aqueous Lliquids and from Supercritical Fluids*. International Conference on Silica, Mulhouse France, September 3-7, 2001. (Invited)

7. S. Ma, R. H. Jackson, B. G. Frederick, *Effect of Surface Reduction on Decomposition of Dimethyl Methyl Phosphonate on Tungsten Trioxide Surfaces*, 48th International Symposium of the American Vacuum Society, San Francisco, California, Oct.28, 2001.

8. S. Ma, F. G. Amar and B. G. Frederick, *Adsorption and Desorption of Methanol on WO₃ (100) Surfaces*, 49th International Symposium of the American Vacuum Society, Denver, Colorado, Oct 28-Nov 2, 2001.

9. R.J. Lad, *Charge Transport Mechanisms in Epitaxial Tungsten Oxide Films Used for Chemiresistive Sensors*, 48th International Symposium of the American Vacuum Society, San Francisco, CA, Oct. 29, 2001.

10. C.P. Tripp, *Silane Chemistry for Selective Detection*, Seton Hall University, Nov 20, 2001.

11. L. Doucette, F. Santiago, S. Moran, R.J. Lad, *Tungsten Oxide Chemiresistive Films Integrated onto Silicon by Use of an Epitaxial BaF₂ Buffer Layer*, 2001 Fall Meeting of the Materials Research Society, Boston, MA, Nov. 26, 2001.

12. R.J. Lad, *In-Situ Conductivity and Hall Effect Characterization of Tungsten Oxide Thin Films*, 2001 Fall Meeting of the Materials Research Society, Boston, MA, Nov. 28, 2001.

13. S.M. Kanan, and C.P. Tripp, *Prefiltering Strategies for Metal Oxide Based Sensors: Use of Chemical Displacers to Selectively Cleave Adsorbed Organophosphonates from Silica Surfaces*, ACS National Meeting, Orlando FL April 1-5, (2002).

14. S.M. Kanan, and C.P. Tripp, *A Comparative Study of the Adsorption of Chloro and Methyl Containing Organophorous Compounds on Nano-Sized Monoclinic and Mesoporous WO₃ Powders*, ACS National Meeting, Orlando FL April 1-5, (2002).

15. R.S. Pilling, S. Ma, A. El Madi, A. Martin, G. Bernhardt, R. J. Lad, B. G. Frederick, *Methods for Compound Classification in Metal Oxide Sensor Array Systems"*, AVS Topical Conference on Understanding and Operating in Threat Environments, Monterey, CA May 1-2, 2002.

16. R.J. Lad, *Chemiresistive Metal Oxide Films on Sapphire and Silicon Substrates for Chemical Agent Detection*, AVS Topical Conference on Understanding and Operating in Threat Environments, Monterey, CA, May 1, 2002.

17. C.P. Tripp, A. Waghe and S.M. Kanan, *New Materials and Strategies for the Selective Detection of Nerve Agents in Semiconducting Metal Oxide Based Sensing*, AVS Topics Conference on Understanding and Operating in Threat Environments, Monterey CA, May 1-2, 2002 (poster)

18. R.J. Lad, *Heteroepitaxy of Tungsten Oxide Films on Sapphire and Silicon for Chemiresistive Sensor Applications*, IEEE International Conference on Sensors, Orlando, FL, June 14, 2002 (Invited)

19. R.S. Pilling, C. S. Kim, S. C. Moulzolf, G. Bernhardt, B. G. Frederick, *Selectivity toward organophosphorous compounds in SMO chemiresistive sensors*, 9th International Meeting on Chemical Sensors, Boston, MA, July 7-10, 2002

20. R. S. Pilling, J. Duncan, B. G. Frederick, *A GC/MS Based Gas-Delivery System for Quantifying Sensitivity and response Time of Gas Sensors*, 9th International Meeting on Chemical Sensors, Boston, MA, July 7-10, 2002.

21. A. L. Martin, R. S. Pilling, L. J. LeGore, B. G. Frederick, *Detection of Nitric Oxide Using Silver and Gold Modified WO_3 Chemiresistive Sensors*, 9th International Meeting on Chemical Sensors, Boston, MA, July 7-10, 2002.

22. L. Doucette, F. Santiago, S. Moran, R.J. Lad, *Use of Insulating BaF_2 Buffer Layers to Integrate Chemiresistive Metal Oxide Sensing Films onto a Silicon Substrate*, 9th International Meeting on Chemical Sensors, Boston, MA, July 9, 2002.

23. A. El Madi, B.G. Frederick, R.J. Lad, *Interaction of Ultra-thin CuO Layers on WO_3 Chemiresistive Sensing Films*, 2002 Fall Meeting of the Materials Research Society, Boston, MA, Dec. 2, 2002.

24. R.J. Lad, *Heteroepitaxial Tungsten Oxide Chemiresistive Sensing Films Containing Nanostructured Catalytic Particles*, 27th Annual Cocoa Beach Conference on Advanced Ceramics & Composites, Cocoa Beach, FL, Jan. 28, 2003.

25. B. G. Frederick, *Role of materials properties in WO_3-based thin film sensor development*, Topical conference on Oxide-Based Chemical and Biological Sensors, 105th Annual Meeting American Ceramic Society, Nashville, TN April 28-29, 2003. (Invited)

PATENTS:

S.K. Kanan and C.P. Tripp, *Selective Filtration and Concentration of Toxic Nerve Agents*, Patent Application Serial No. 10/001,664
Filed October 23, 2001